

1N-14287

NASA Contractor Report 178114

THE INFLUENCE OF DEFECTS ON THE FATIGUE RESISTANCE OF BUTT AND GIRTH WELDS IN A106B STEEL

B. N. Leis, D. P. Goetz and P. M. Scott

(NASA-CR-178114) THE INFLUENCE OF DEFECTS
OF THE FATIGUE RESISTANCE OF BUTT AND GIRTH
WELDS IN A106B STEEL Final Report (Battelle
Columbus Labs., Ohio.) 108 p HC A06/MF A01

N86-28166

CSCL 11F G3/26

Unclas
43398

**BATTELLE COLUMBUS DIVISION
COLUMBUS, OHIO**

**Contract NAS1-17404
JULY 1986**



National Aeronautics and
Space Administration

Langley Research Center
Hampton, Virginia 23665

~ ~

~ ~

INTRODUCTION

The goal of this program was to develop a rationale for accepting welds containing workmanship-based, code-rejectable defects. This development was planned to evolve through three phases. In the first phase, the technical literature was assembled and reviewed to determine the effects of planar and volumetric defect indications on fatigue behavior. The purpose of the second phase was to sequentially generate fatigue life data in A106 Grade B steel in flat plate, pipe segment, and pipe section test geometries containing a variety of artificial and natural defects. The third phase was to generate acceptance criteria based on the data of the second phase, consistent with the results of the literature search. The viability of the acceptance criteria was contingent on the availability of an appropriate literature data base.

Activities in the first phase were designed to generate preliminary acceptance criteria for volumetric and planar indications. To that end, a literature search was initiated looking for data documenting the effect of defect size and shape on fatigue (not fracture) behavior of welds. The literature search was followed by a telephone and telex campaign, and the mailing of a detailed questionnaire. The campaign covered European, British, Canadian, Japanese and American Laboratories. Provisions were made to visit prominent laboratories based on the responses to the campaign. As detailed in Appendix A, which highlights the effort of Phase I, the response to all facets of the literature campaign was sparse. Significantly useful responses were received only from CANMET and the University of Illinois.

Activities in Phase II were directed at developing application-specific data in a format that permitted interpretation of the factors controlling fatigue life of weldments containing known defects. The contract called for the performance of ten tasks to provide a skeletal database that could be used to make decisions on defect acceptance. This database, when supplemented with the anticipated literature data, was to form the basis for developing defect acceptance criteria. This criteria development was planned for Phase III. The plan was to use Linear Elastic Fracture Mechanics (LEFM) state-of-the-art calculations to consolidate the total database. Thereafter, criteria would be developed by interpolation and limited extrapolation based on the LEFM analysis. The limited response to the Phase I survey was seen as limiting the scope and veracity of the criteria to be developed. However, provided that LEFM could consolidate the data and could be used to independently predict observed results, the program's goal would not be jeopardized for NASA's specific application.

This report presents the efforts in Phase II and III of this program. The experimental effort in Phase II is set forth in sections titled: Experimental Program; Experimental Details; and Results. Efforts directed at developing criteria as a part of Phase III are presented in the section titled Discussion. The report closes with a Summary of the Efforts in Phase II and III, and the Conclusions.

EXPERIMENTAL PROGRAM

Overview

The objective of this study was to develop data which, with the aid of fatigue data in the literature, would lead to the development of acceptance guidelines for welds with code-rejectable defects. LEFM was to be used as an interpolative tool in combining literature data and the results of this program's experiments.

Throughout the program, emphasis was placed on understanding the effect of specimen and flaw design on defect growth behavior. Such an understanding is needed not only to interpret existing data, but also in the design of future tests. By using material, welding practices, etc., similar to that used in the NASA LaRC physical plant, a tie was made to the particular service situation of interest. In view of the service of interest, the program focused on girth butt welds made using a backup ring, and considered the effects of pressure cycling only. It is possible that defective welds either made without using backup rings, or subjected to primary, or even secondary, bending would behave differently than those studied herein, particularly for the vessel tests.

In keeping with the programs purpose of isolating the effect of defects and the need to demonstrate the viability of LEFM to characterize the evolution of defects, all welds were normalized to reduce data scatter and uncertainties in data analyses associated with variable, unknown residual stress levels and weld-induced residual stresses.

In order to meet the objective, several questions were addressed. These questions explored four facets of the program objective as it related to data development. The facets explored were: specimen geometry; defect type and simulation; defect characterization; and defect growth. The specific questions asked were:

- What specimen geometry is appropriate for determining the fatigue performance of pipe girth welds? Four specimen geometries involving butt or girth welds with backup rings were tested: flat plates and pipe wall segments (made by cutting a pipe lengthwise so that a plate with curvature in the width direction was produced) which were subjected to alternating tensile loads; and pipe segments (made by welding end caps on a segment of pipe to make a pressure vessel) and actual pipe segments with complex geometries taken from service which were subjected to pressure cycles.
- What type of weld defect can be used to simulate the service situation? Three types of flaws were considered: artificial flaws made by the electrical discharge machining (EDM) process, natural defects intentionally induced by control of the welding process, and defects in pipes removed from service. Two general geometries were examined: planar (representing lack of fusion and lack of penetration) and volumetric (representing slag and porosity).
- How do non-destructive inspection (NDI) data help in determining the fitness-for-purpose of welds with

code-rejectable defects? NDI data were taken for specimens with natural weld defects in order to examine their usefulness in this regard.

- How can linear elastic fracture mechanics (LEFM) crack growth calculations be used to supplement and interpret the experimental data? It was anticipated that LEFM could be used to interpolate between experimental data.

Elements of the Plan for Comparative Experiments

The experimental program consisted of a series of comparative experiments. Stress versus fatigue-life curves were developed for several combinations of specimen geometry, flaw type and flaw size to help explore the above listed questions. Comparison of these curves allows isolation of the effects of each variable. A small number of reference experiments also were done to develop data which allowed interpretation of the fatigue life data using LEFM-based crack propagation calculations. To further aid in understanding the test results, the fracture surfaces also were examined.

Table 1 presents the anticipated test matrix for the comparative experiments. The left-most column gives the specimen geometry; the remaining columns detail the flaw type and test conditions. Each entry in Table 1 represents a series of four load controlled fatigue-life tests which form a stress-versus-life (S-N) curve. The stress levels were chosen so that three specimens failed between 10^4 and 10^6 cycles while the fourth was at a fatigue endurance threshold (for growth) stress level at 2×10^6 cycles. Stress levels were chosen within the range of stresses considered realistic in light of ANSI B31.3.

TABLE 1. ANTICIPATED TEST MATRIX FOR COMPARATIVE EXPERIMENTS

SPECIMEN GEOMETRY	FLAW TYPE			
	ARTIFICIAL FLAW(a)		NATURAL FLAW(b)	SERVICE FLAW
Flat Plate	<u>R = 0.01</u>			
	small	small		
	planar	volumetric		
	large	large		
	planar	volumetric		
	<u>High Stress Ratio(c, d)</u>			
Wall Segment(e,f)	planar	volumetric	planar	volumetric
Pipe Segment(f)	planar	volumetric	planar	volumetric
Pipe from Service				extant flaws(g)

Notes:

- (a) All artificial flaws made by EDM process.
- (b) All natural flaws made by control of the welding process.
- (c) Anticipated stress ratio $R = 0.8$; all other tests to be run at $R = 0.01$.
- (d) EDM flaw type to be determined during course of program.
- (e) EDM defects to be chosen from sizes used in flat plates.
- (f) Each entry represents four tests which determine a stress-versus-life curve.
- (g) Eight tests to be performed.

TABLE 2. FINAL TEST MATRIX FOR COMPARATIVE EXPERIMENTS

SPECIMEN GEOMETRY	FLAW TYPE			
	ARTIFICIAL FLAW(a)		NATURAL FLAW(b)	SERVICE FLAW
Flat Plate	<u>R = 0.01</u>			
	small	small		
	planar	volumetric		
	(8 tests) (3 tests)			
	<u>R = 0.01</u>			
	large	large		
	planar	volumetric		
	(5 tests) (1 tests)			
	<u>R ≠ 0.01 (c)</u>			
	spot checks on R			
	(3 tests at $R = .4$)			
	(2 tests at $R = .6$)			
Wall Segment	planar		planar	volumetric
	(7 tests)		(5 tests)	(5 tests)
Pipe Segment	planar	volumetric	planar	
	(4 tests)	(4 tests)	(4 tests)	
Pipe from Service				extant flaws
				(2 tests - multifiawed specimens)

Notes:

- (a) All artificial flaws made by EDM process.
- (b) All natural flaws made by control of the welding process.
- (c) All other flat plate and wall segment tests run at $R = 0.01$; all pipe tests run at 0.1.

During the course of testing, several unexpected results led to a redirection of the experimental program. First, it was found that flat plate specimens with reinforcement would not fail at an EDM defect in the weld. Instead, a crack would form at the toe of the weld reinforcement even though no code-rejectable undercut was present. It was found that, if an EDM flaw was cut through a backup ring and into the weld, the crack starting from the flaw would be pinned by the unstressed backup ring. These unanticipated results led to adjustment of some tests, redesign of some flaws, and reduction of the effort, as noted in the section on experimental details. A third cause for change in the anticipated test matrix concerned the volumetric EDM flaws. Several tests were done using flat plate specimens. The failures clearly did not represent the behavior of natural volumetric weld defects such as porosity or slag. Therefore, the remaining flat plate and wall segment specimens were directed to examining planar EDM defects. Fourth, the stress ratio used for the high stress ratio tests of flat plate specimens with artificial defects (cf. Table 1) was lowered from $R = 0.8$ to 0.6 and then 0.4 to produce failures at reasonable stresses and lives. Fifth, difficulties in producing fatigue failures at natural volumetric defects in pipe wall segment specimens indicated that failures could not be produced in pipe segment specimens with volumetric defects at reasonable lives and stresses. Therefore, those tests were dropped.

The final experimental program is given in Table 2. Note that it does not list the reference experiments added to the program to aid in data analysis and interpretation.

Reference Experiments

Reference experiments were added to the matrix to assist in design of flaws and to allow the use of LEFM in interpreting the results of the comparative experiments. One flat plate specimen was used to get an estimate of the threshold stress intensity range, ΔK_{th} , and to develop fatigue crack growth rate data for weld metal. A second flat plate specimen was used to check the EDM flaw design to be used to simulate small planar weld defects to ensure that it would grow at a reasonable stress and produce a fatigue life in the desired range. A third reference experiment was conducted to assess the amount of induced bending associated with the wall segment specimens. The bending was quantified by performing a strain survey on a strain gaged pipe wall segment specimen covering a range of crack lengths. The last reference experiment was a check on the crack shape as it changed during the course of a fatigue test.

EXPERIMENTAL DETAILS

Material Characterization

Most of the specimens tested as part of this program were fabricated from four joints of 203 mm (8-inch) nominal diameter Schedule 40 (8.18 mm [0.322-inch] nominal wall thickness) ASTM A106 Grade B seamless pipe. All four pipe joints were from the same heat. The heat number was 83795. The remaining specimen consisted of 76 mm (3-inch) nominal diameter

Schedule 40 pipe segments which were removed from service from the NASA Langley Research Center. NASA records indicate it was A106 Grade B pipe, vintage early 1950's. Chemical analyses were made for each of the four joints of 203 mm (8-inch) nominal diameter pipe. Table 3 presents the results of those analyses. No analysis was done for the pipe removed from service.

Tensile (flattened) strap specimens were machined from both the longitudinal and transverse directions of each of the four joints of pipe in the as-received condition. In addition, since all of the specimens were normalized (to reduced residual stresses) prior to testing, tensile strap specimens were also machined from pipe sections subjected to the same normalizing treatment as the welded specimens. The specimens were normalized by heating them to 870 C (1,600 F) for 30 minutes, and allowing them to air cool. Note, only longitudinally oriented normalized specimens were tested, since the mechanical properties in the longitudinal direction are most important for this program. Table 4 presents the results of the tensile tests for each of these pipe joints. Also included in Table 4 are the specified minimum mechanical properties for ASTM A106 Grade B pipe. The mechanical properties for each of the pipe joints exceeded the specified minimum value.

Micrographs (100 x magnifications) were made to document the microstructure of the base metal in the normalized condition. Micrographs were taken at different locations in different orientations. Little difference in the microstructure was observed for the different orientations and locations. Figure 1 shows views of the typical microstructure taken in the L-T direction, at mid-thickness and at the surface. These views are typical of normalized steel showing a mix of ferrite and pearlite and evidence

TABLE 3. RESULTS OF CHEMICAL ANALYSIS FOR EACH OF THE FOUR PIPE JOINTS

Pipe Joint	C	Mn	P	S	Si	Cu	Sn	Ni	Cr	Mo	Al	V	Cb	Zr	Ti
1	0.20	0.78	0.008	0.015	0.28	0.19	0.011	0.15	0.18	0.042	0.024	0.000	0.000	0.000	0.001
2	0.26	0.78	0.009	0.018	0.30	0.19	0.012	0.15	0.17	0.047	0.026	0.000	0.001	0.000	0.001
3	0.20	0.80	0.008	0.016	0.29	0.19	0.011	0.15	0.18	0.042	0.026	0.000	0.000	0.000	0.001
4	0.26	0.79	0.010	0.020	0.38	0.19	0.013	0.14	0.17	0.050	0.030	0.001	0.003	0.000	0.001
	B	Co	W	Pb											
1	0.0000	0.006	0.00	0.00											
2	0.0000	0.007	0.00	0.00											
3	0.0000	0.006	0.00	0.00											
4	0.0000	0.007	0.00	0.00											

TABLE 4. RESULTS OF TENSILE TESTS FOR EACH OF THE FOUR 203 MM (8-INCH) DIAMETER PIPE JOINTS

As Received - Transverse Orientation					As Received - Longitudinal Orientation			
Pipe Joint	2 Percent Offset Yield Strength, MPa (ksi)	Ultimate Strength MPa (ksi)	Percent Elongation 25.4 mm (1-Inch) Gage Length		2 Percent Offset Yield Strength, MPa (ksi)	Ultimate Strength MPa (ksi)	Percent Elongation 25.4 mm (1-Inch) Gage Length	
1	389 (56.7)	583 (84.8)	24.5		354 (51.5)	578 (84.2)	32.0	
2	400 (58.3)	578 (84.2)	17.5		363 (52.8)	578 (84.2)	32.6	
3	366 (53.3)	594 (86.5)	24.9		385 (56.1)	581 (84.6)	32.7	
4	365 (53.1)	585 (85.1)	26.2		357 (52.0)	571 (83.2)	31.0	
Average	380 (55.3)	585 (85.1)	23.3		365 (53.1)	577 (84.0)	32.1	
Normalized - Longitudinal Orientation					Specified Minimum - ASTM A106B			
Pipe Joint	2 Percent Offset Yield Strength, MPa (ksi)	Ultimate Strength MPa (ksi)	Percent Elongation 25.4 mm (1-Inch) Gage Length	Direction	2 Percent Offset Yield Strength, MPa (ksi)	Ultimate Strength MPa (ksi)	Percent Elongation 25.4 mm (1-Inch) Gage Length	
1	343 (50.0)	537 (78.2)	34.2	Transverse	240 (35.0)	412 (60.0)	16.5	
2	343 (50.0)	545 (79.3)	32.5	Longitudinal	240 (35.0)	412 (60.0)	30.0	
3	355 (51.7)	546 (79.5)	35.6					
4	339 (49.4)	538 (78.4)	37.5					
Average	345 (50.3)	542 (78.9)	34.9					

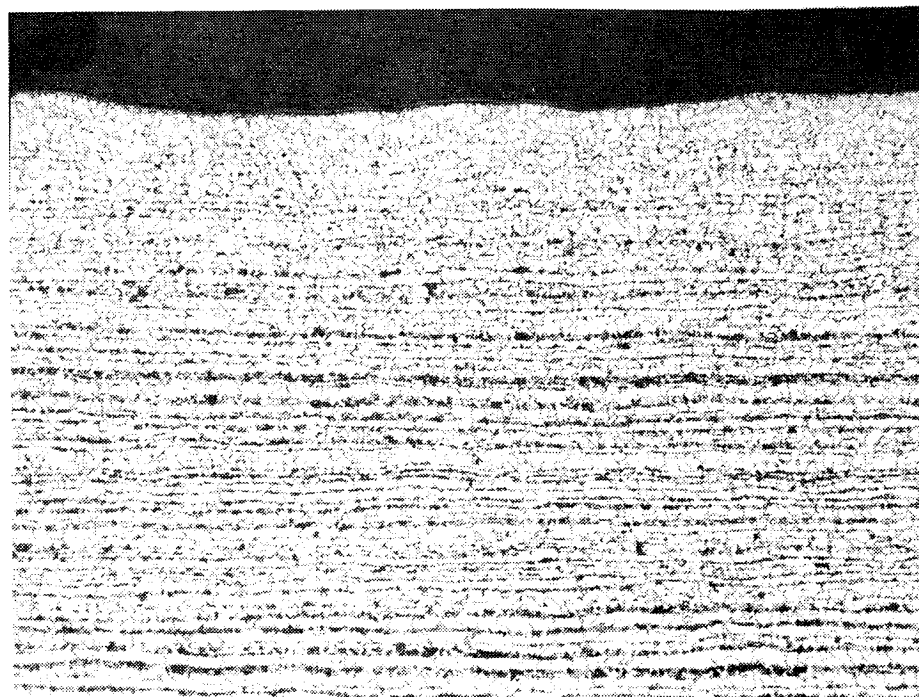


100x

Nital

IM390

a. L-T direction at mid thickness



100x

Nital

IM389

b. L-T direction at the surface

FIGURE 1. MICROSTRUCTURE OF THE BASE METAL IN THE
NORMALIZED CONDITION

of a structure aligned by hot-rolling. There is some evidence of slight grain growth and decarburization to a depth of about 100 μm (0.004 inch). Some nonmetallic inclusions are evident.

Welding Procedures and Details of Weld Defects

Four basic types of defects were evaluated as part of this program: artificial planar, artificial volumetric, natural planar, and natural volumetric. All of the artificial defects were introduced into quality (code acceptable) welds using electrical-discharge-machining (EDM) techniques. These welds were made using shielded metal arc welding and E7018 electrodes with backup rings in place. Subsequent to the welding operation, some welds were subjected to an ultrasonic and radiograph inspection. All of the "quality welds" successfully passed both inspections, subject to AWS D1.1.

Several procedures for introducing natural defects were tried using small samples welded with different techniques. The suitability of the technique was then assessed by inspecting the welds both ultrasonically and radiographically for evidence of flaws. In addition, discussions were held with representatives of a number of organizations. GARD, INC., the Welding Institute of Canada, and the Welding Engineering School of Ohio State University volunteered their ideas on acceptable procedures for introducing natural defects.

For planar flaws the agreement between parties as to how to simulate natural defects was generally good. For an incomplete- or lack-of-penetration (LOP) defect, a tight fitup with a slightly larger-than-normal root face worked well. For lack of fusion (LOF), allowing the weld deposit to build up

on one side was noted to work well, especially if a zinc-oxide mold-release compound is painted on one side of the joint.

For volumetric flaws, the agreement between parties was not so evident. Slag pockets were easy to produce in that slag could be introduced by not cleaning the weld in between weld passes. However, slag was not our preference for a volumetric weld defect; porosity was. Porosity tends to be a more rounded defect than slag. Consequently, the sharpening or crack initiation period should be longer for porosity than for slag. Therefore, it was thought that the lives associated with a slag-type defect would lie somewhere in between a planar and a more rounded (porosity) type defect. Based on the program's desire to bound defect behavior, porosity was our first preference for a volumetric defect.

There was much disparity among the several methods suggested for introducing porosity. Much of the disparity revolved around the introduction of foreign matter. For those that believed that foreign matter did not create secondary problems, the production of porosity was easy. However, several argued that the foreign materials commonly used, such as sulfur, iron filings, or oily substances, can upset the weld chemistry. Furthermore, to obtain the gross amount of porosity called for in the study, it would be necessary to use a large amount of foreign substance. This would not only produce porosity but also it would produce slag and possibly some cracking that would confuse interpretation. For this reason, most individuals felt that the local use of the gas-metal-arc-welding (GMAW) process offered the most promise. This process may be upset easily by reducing the gas flow rate significantly to produce porosity without introducing slag or cracking. Accordingly, the

porosity defects were made by intentionally upsetting the welding parameters by reducing the CO₂ flow rate to less than 1 CFH during gas-metal-arc-welding in the area where the defect was desired. The defected area was surrounded by code acceptable weld metal.

After introducing the planar and volumetric natural defects, the welds were inspected both ultrasonically and radiographically.* Table 5 presents the results of the radiograph inspections for the welds with the natural defects.

Specimens

Flat plate specimens. The specimen design used in the flat plate tests is shown in Figure 2. The material used was described above. The 203 mm (8-inch) pipe was cut to length, then cut lengthwise into two halves, flattened, and then normalized to relieve the flattening stresses. The flattened plates were saw cut at the locations for the welds, and the edges were beveled in preparation for welding. Flattened backup rings were used in making the welds. All of the welds were inspected and found to be code-acceptable welds. The specimens were then normalized again. During the normalization, the specimens were stacked in an oven with the ends unsupported. As a result, some of the ends drooped during heating. The specimens were then normalized again.

* Seven samples were inadvertantly omitted: FPA-S-16, 17, 18; and CPN 6, 7, 9, 10.

TABLE 5. RESULTS OF THE RADIOGRAPH INSPECTIONS FOR THE WELDS WITH THE NATURAL DEFECTS

WCI SPECIMEN I.D.	BCL SPECIMEN I.D.	ACCEPT	REJECT	LACK OF PENE.	LACK OF FUSION	POROSITY	SLAG	UNDERCUT	REMARKS	RADIOGRAPH I.D.
32V1	CPN-2		X			X				32V1-4/0-1
32V2	CPN-4		X			X				32V1-4/0-1 & 1-2
32V3	CPN-5		X			X				32V1-4/1-2
32V4		✓								32V1-4/2-3
32P1	CPN-1	✓				✓				#2/0-1
32P2			X			X				#2/0-1 & 1-2
32P3	CPN-3		X			X				#2/1-2
32P4			X			X	X			#2/2-3
54P1	54P1		X			✓	X	✓	1st Insp.-5/16/84	54P1
54P2	54P2		X			✓	X	✓	"	54P2
54P3	54P3		X	X		✓	X	✓	"	54P3
54P4	54P4	✓				✓	✓	✓	"	54P4
54P1	54P1		X		X	✓		✓	2nd Insp.-5/31/84	54P1
54P2	54P2		X			X	✓	✓	Same Level II Insp	54P2
54P3	54P34		X	X		X	X		As Did the 1st Insp.	54P3
54P4	54P4		X			✓	X	✓		54P4

TABLE 6. RESULTS OF THE RADIOGRAPH INSPECTIONS FOR THE WELDS IN THE TWO 76 MM (3-INCH) DIAMETER SPECIMENS(a)
(Radiograph identification number is the same as the weld identification)

NASA WELD IDENTIFICATION	ACCEPT	REJECT	LACK OF PENE.	LACK OF FUSION	POROSITY	SLAG	UNDERCUT	BURN THROUGH	MELT THROUGH	ROOT CONCAVITY	REMARKS
1-1	✓								✓		At Butt Ring
1-2		X		X							
1-3	✓										
1-4		X				X					
1-5		X				X					
1-6	✓				✓				✓		
1-7	✓										
2-1	✓										
2-2		X		X		X					
2-3		X	X		✓		✓				
2-4		X		X	✓			✓	✓		
2-5		X			✓	X					
2-6		X		X		X					
2-7	✓				✓					✓	
2-8		X			✓	X					
2-9	✓										
2-10	✓										

(a) A check mark indicates an acceptable weld based on the lack of detectable indications or the presence, of code acceptable indications: A cross mark denotes corresponding code rejectable indication.

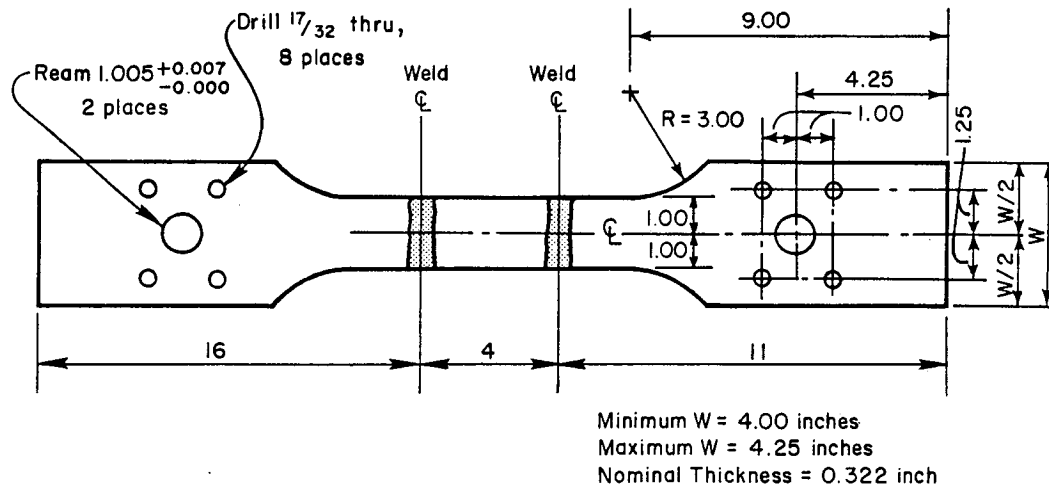


FIGURE 2. FLAT PLATE SPECIMEN DESIGN

This necessitated straightening those ends. Care was taken not to bend the welds or center section during straightening. Finally, machining was done to finish the specimens.

Four artificial flaws were used. The two planar flaws were geometrically similar, but of different sizes. Both were semi-elliptical surface flaws with an aspect ratio of depth to semi-length (a/c) of $2/3$. The depth of the small flaw was 2.5 mm (0.1 inch); the depth of the large flaw was 5.1 mm (0.2 inch). The two volumetric flaws have the same depths as the planar flaws. They were semi-ellipsoidal in shape, with the shape and size identical to the 5.1 mm (0.2 inch) planar flaw rotated about an axis perpendicular to the specimen's surface. That is, artificial volumetric flaws were blind holes with curved bottoms, with an aspect ratio (a/c) of $2/3$ in the plane of the specimen.

The flaws were made in sound welds by cutting through the backup ring and into the weld at the mid-width of each specimen. The depth was referenced to the surface of the specimen and not to the surface of the backup ring (see Figure 3). Electrodes, 0.254 mm (0.010 inch) thick which had tapered edges, were used to make the sharp-tipped planar flaws.

Early in the testing, it was discovered that the unstressed backup ring could "pin" the crack. This is illustrated by the fracture surface shown in Figure 4. Because this complex growth would confuse subsequent data interpretation, the backup rings on the remaining specimens were cut by EDM by using a flat electrode with a curved edge (a 76 mm (3-inch) radius). Figure 5 shows an example of the result as seen on a fracture surface. The backing ring was cut so as to "unpin" the defect by cutting to nearly intersect the defect at the surface of the specimen. Thus, care was taken to make the cut 0.127 - 0.254 mm (0.005-0.010 inch) shallower than the thickness of the backup ring to ensure that the weld metal was not cut.

In addition, it was also discovered early in the testing that a crack could initiate at the toe of the weld reinforcement and cause failure before an EDM planar flaw could grow to failure. In order to force the specimens to fail at the desired location, a hand grinder was used to increase (blend) the radius at the toes of the weld reinforcement on the rest of the specimens.

Pipe wall segment specimens. The specimen design used in the pipe wall segment tests is shown in Figure 6. Pieces of pipe were first cut to the proper length. They were then cut into two equal lengths. The edges of the

ORIGINAL PAGE IS
OF POOR QUALITY

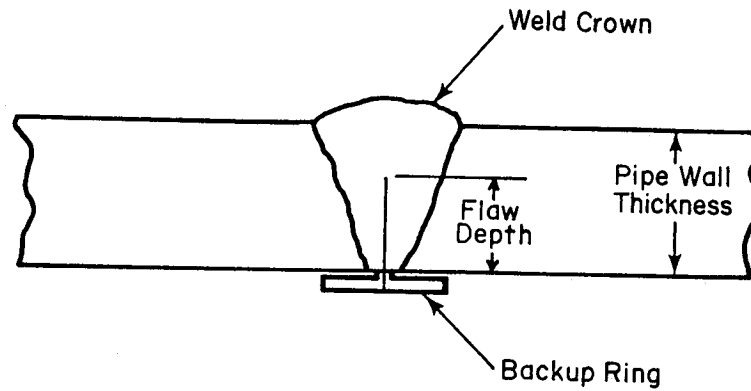
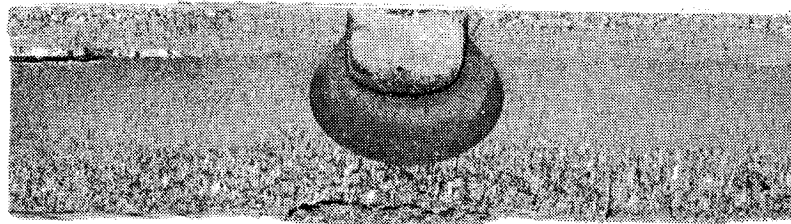


FIGURE 3. REFERENCE FOR MEASURABLE FLAW DEPTH FOR EDM FLAWS



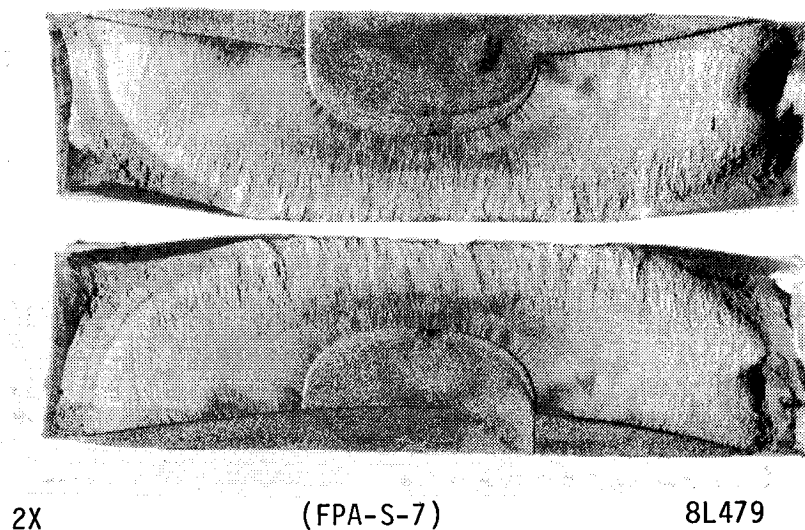
2X

(FPA-S-2)

IM462

FIGURE 4. FRACTOGRAPH ILLUSTRATING CRACK PINNING BY THE BACKUP RING
(Note: EDM flaw is cut through ring with its position referenced to the surface of the plate, as if the backup ring did not exist.)

ORIGINAL PAGE IS
OF POOR QUALITY



For a flat plate specimen

FIGURE 5. FRACTOGRAPH SHOWING EDM FLAWS AND BACKUP RING CUT BY EDM

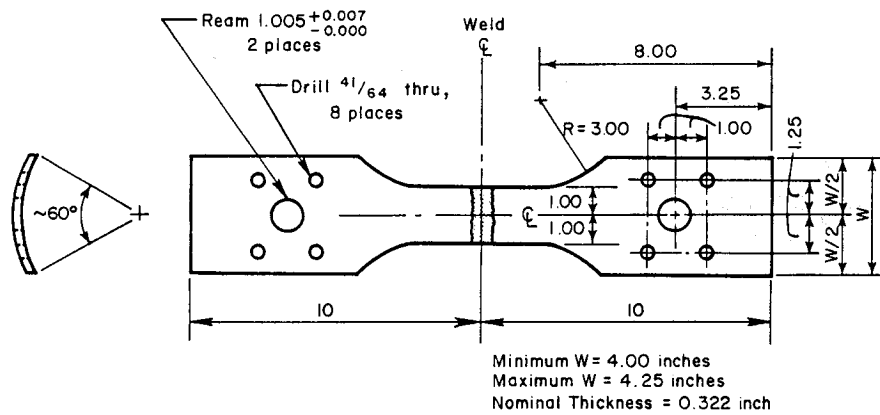


FIGURE 6. PIPE WALL SEGMENT SPECIMEN DESIGN

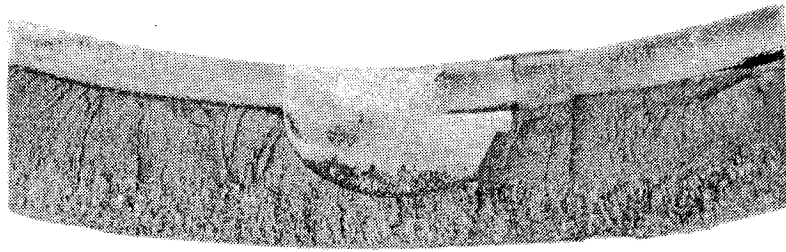
second cut were beveled, and then the two pieces were welded together. Code-acceptable welds were made for specimens to receive artificial (EDM) flaws. Natural flaws were induced by control of the welding process for the remainder (i.e., porosity and lack of fusion). After normalizing, each of the pieces were cut lengthwise into six specimen blanks. These were then machined to the final configuration.

The artificial flaw design used in these tests was the same as for the large planar EDM flaw used with the flat plates, as shown in Figure 7. Again, the maximum depth was 5.1 mm (0.2 inch) referenced from the surface of the specimen. The backup ring for the artificial flaw specimen was cut using a 95.2 mm (3.75 inch) radius EDM electrode. All weld toes were ground as for the flat plate specimens.

Vessel and pipe specimens. A total of 14 vessel or pipe-segment specimens were used in this program. Twelve of the pipe-segment specimens were fabricated from 203 mm (8-inch) nominal diameter pipe. The remaining two specimens were sections of 76 mm (3-inch) nominal diameter pipe removed from the NASA Langley Research Center.

The 203 mm (8-inch) diameter specimens were fabricated as pressure vessels with end caps on each end and a centrally located girth weld as shown in Figure 8. One of the end caps was fitted with a nipple for a pressurization line. The length of the vessels from end cap weld to end cap weld was approximately 610 mm (24-inches). The center girth welds contained an internal surface defect, either an artificial defect in a code-acceptable weld or a natural defect introduced using one of the welding procedures discussed previously.

ORIGINAL PAGE IS
OF POOR QUALITY



2X

(CPA-S-8)

IM459

For a pipe wall segment specimen

FIGURE 7. FRACTOGRAPH SHOWING EDM FLAWS AND BACKUP RING CUT BY EDM

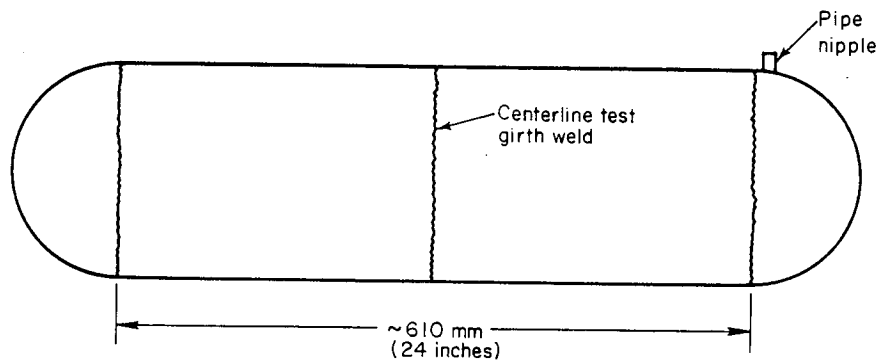


FIGURE 8. SCHEMATIC OF 203 MM (8-INCH) NOMINAL DIAMETER
PIPE-SEGMENT TEST SPECIMEN

The nominal defect size was the same for each of the 12 experiments. The defect extended 120-degrees around the pipe circumference. The depth was approximately 4.95 mm (0.195-inch). This depth was approximately 60 percent of the pipe wall thickness, with an area equal to about 20 percent of the cross section. The depth was referenced to the inside surface of the pipe and not the backing ring (see Figure 3). The size of these defects was chosen on the basis of LEFM estimates that indicated such flaws would grow through the wall thickness in reasonable lives (i.e., similar lives to those in the flat plate and wall segment tests) at code allowable stress levels. For safety considerations the length of the defect was selected so that the failure mode of the defect would be a leak and not a rupture based on a ligament instability analysis. Four of the twelve specimens had an artificial planar type of defect. The defect was introduced using electro-discharge-machine (EDM) techniques. The tip of the electrode was tapered in order to achieve a sharp notch tip as indicated in Figure 9a. Four of the twelve specimens had an artificial volumetric type of defect. This type of defect was introduced using EDM techniques except a wide electrode with a curved blunt tip illustrated in Figure 9b was used. The remaining four specimens had a natural planar defect introduced by the previously discussed methods. Because previous wall segment tests indicated that unrealistic defect sizes or stresses would be required to achieve fatigue lives of interest in this program, pipe-segment specimens with natural volumetric defects were not fabricated.

The two 76 mm (3-inch) diameter specimens were supplied by NASA with end caps already in place. Each specimen contained multiple defective welds.

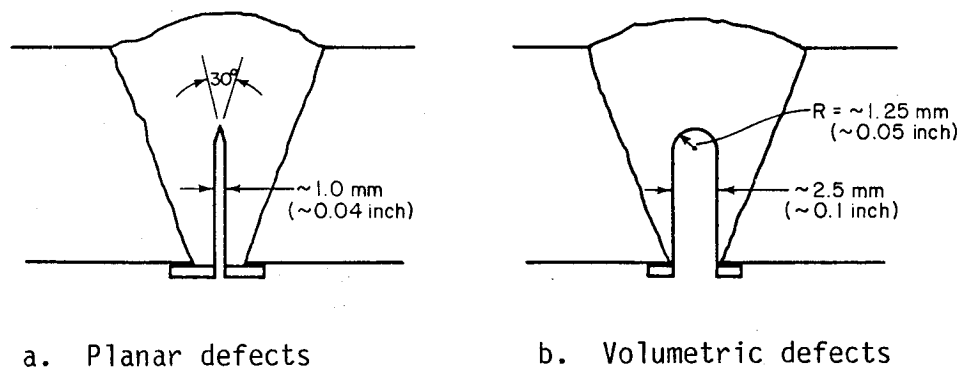


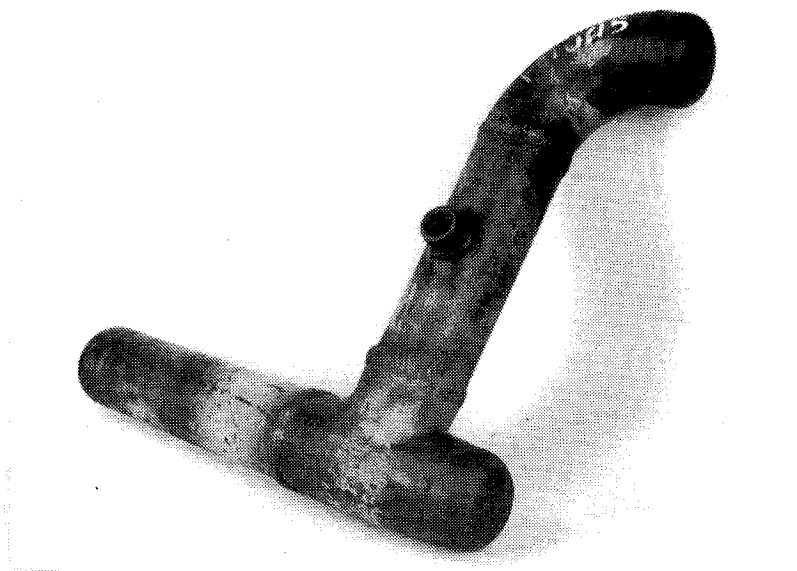
FIGURE 9. DETAILS OF ARTIFICIAL DEFECTS

Table 6 presents the results of the radiographic inspections for the welds in these two 76 mm (3-inch) diameter specimens. These results were supplied by the sponsor. Specimen 1, shown in Figure 10a, contained a pipe tee, a pipe elbow, two short lengths of straight pipe, three end caps, a pipe nipple, three quality end cap welds, and three defective girth welds. Specimen 2 contained a pipe tee, two elbows, two metric joints, two short straight sections of pipe, three end caps, a pipe nipple, three code-acceptable end cap welds, and six defective girth welds.

Equipment

Uniaxial flat plate and wall segment tests. Testing was done in load control using commercially available 111.2 kN (25 kip) and 222.4 kN (50 kip) closed-loop servohydraulic test frames. The forcing function was sinusoidal at frequencies from 1 to 20 HZ. The load cell calibrations are

ORIGINAL PAGE IS
OF POOR QUALITY



7506-6

a. Specimen No. 1



7506-3

b. Specimen No. 2

FIGURE 10. PHOTOGRAPHS OF THE TWO 76 MM (3-INCH) NOMINAL
DIAMETER SAMPLES REMOVED FROM SERVICE FROM
NASA LANGLEY FACILITY PLANT

traceable to the National Bureau of Standards (NBS). Machine alignment was checked using a strain gaged alignment specimen. The pipe wall segment specimens were gripped by using curved inserts, to allow conventional flat plate grips to be used.

Vessel and pipe tests. Testing was done in a containment vessel large enough to hold the test specimens. A schematic of the facility is shown in Figure 11. Tests were conducted in closed-loop pressure control to a sinusoidal waveform at a frequency of 1 Hz. Hydraulic oil was used as the pressurizing medium. The calibration of the pressure transducer was traceable to NBS. Two different systems were used to detect failure and shutdown the facility. A flapper-type switch was positioned directly over the centerline of the flaw such that if the flaw broke through the wall, and resulted in a pin-hole leak, the resulting jet of oil would contact the flapper, activate the switch, and shutdown the system. The second system was a float device such that when the oil in the vessel escaped through the resulting through-wall flaw, the oil level in the containment vessel rose, activating the float device, and shutting down the system.

Procedure

Comparative uniaxial tests (flat plates and wall segments). The same basic test procedure was used for the uniaxial specimens for comparative tests. The tests were run in load control using a sinusoidal command function. Failure was defined as separation of the specimen into two pieces. After failure, the fracture surfaces were preserved for inspection.

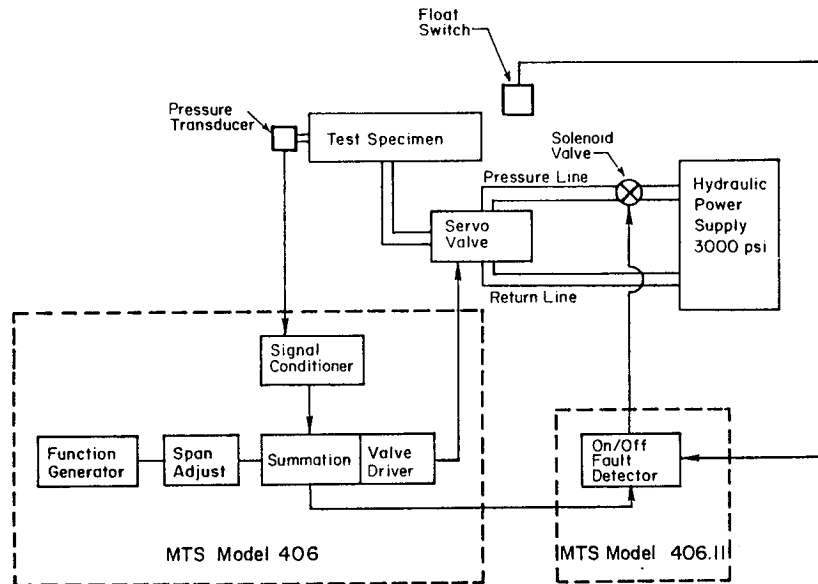


FIGURE 11. SCHEMATIC OF THE VESSEL AND PIPE TEST LOOP

Two pipe wall segment specimens produced unexpected results due to errors in manufacture. One specimen was tested which had the backup ring cut, but had no flaw. A second specimen was tested with a cut which extended through the backing ring and about 0.5 mm (0.02 inch) into the weld. This cut caused premature failure of the specimen.

Comparative vessel and pipe tests. Vessel specimens were plumbed into the pressure cycling containment facility and cycling commenced. Cycling continued until one of the crack detectors tripped, stopping the cycling.

In several early experiments the end-cap quality welds cracked prior to the defective centerline girth welds. This premature cracking of the end cap welds was attributed to residual stresses. In order to prevent such cracking in the vessel specimens, they were normalized after welding to relieve residual stresses. Subsequent to the normalization process,

pressurization nipples were welded onto one of the end caps. The above noted cracking occurred in the vicinity of this nipple. The problem was resolved in the later experiments, by local stress relief with a torch in the area surrounding these nipples. The weld region was heated to approximately 669 C (1200 F) [cherry-red glow], and held at that temperature for approximately 20 minutes. With one exception, all specimens which had been locally stressed relieved failed in the center girth weld. The one exception was a natural planar type of defect. This specimen was subjected to 1,337,850 cycles prior to failing in an end cap weld.

The procedures used for the 76 mm (3-inch) diameter pipe tests was the same as that for the 203 mm (8-inch) diameter experiments except that only the float interlock switch was used to shutdown the system. Due to the multiple flaws, it was impractical to use the flapper type device. Additionally, each of the end cap welds and nipple welds was locally stressed relieved with a torch using procedures similar to those used for the later 203 mm (8-inch) diameter experiments.

Reference tests. Crack growth data were developed using a flat plate specimen with quality welds (Figure 2). Unlike the specimens used for the comparative experiments, both sides of the specimen were ground flat. The backup ring and weld reinforcement were completely removed. An EDM flaw was cut completely through the thickness at the mid-width on both welds forming a center cracked panel. A Krak gage was mounted at each of the eight surface flaw tips. An automated data acquisition system was used to collect crack growth data during the test. The specimen was cycled in a load control mode

using a sinusoidal waveform at a stress ratio of 0.1 and a frequency of 33 Hz. Initially the load range was incremented 12.5 percent every 30,000 cycles until a growth rate above 2.54×10^{-6} mm/cycle (1×10^{-7} inch/cycle) was reached. The load range was then decremented by 8 percent every 30,000 cycles until a growth rate of 1.5×10^{-6} mm/cycle (6×10^{-8} inch/cycle) was reached. The load was then held constant until one of the cracks grew to failure.

A second reference test involved a design check of the small artificial planar defect which was used during the comparative tests. The welds and backing ring of a flat plate specimen were ground flush. A small EDM flaw like that described for the comparative tests (depth of 2.54 mm (0.1 inch) and aspect ratio of 2/3) was made in both welds. The specimen was cycled at $R = 0.01$ at a stress range estimated to cause near threshold growth based on the through crack data. Crack gages were again used to measure the surface crack growth. Failure of the specimen at 2,234,900 cycles (cf. the desired threshold lifetime of 2×10^6 cycles) verified the viability of the flaw design and gave direction about what stress levels should be used in subsequent comparative testing.

A third reference test involved measuring bending strain distributions as a function of crack length. Calculations of the bending stress in the test section showed that the amount of bending was highly dependent on the resistance of the grips to rotation. For this reason, a strain gaged specimen was used to quantify the amount of bending strain for the test fixtures. Measured bending strains were negative on the convex side of the specimen and positive on the concave side. The ratio of bending strain to axial strain at midwidth on the concave side (near where the artificial flaws were cut) was

1-to-10 or less. However, at the mid-width of the convex side the ratio varied from 3-to-10 to 2-to-5. Strain readings at other points revealed that the maximum ratio for any point on the cross section was about 2-to-5, over the range of crack sizes of interest. This strain survey data is used to correct nominal stresses as discussed later in the data analysis section.

The final reference experiment provided data to help in evaluating the viability of LEFM crack propagation calculations for purposes of data interpretation and analysis. A pipe wall segment specimen with a 5.1 mm (0.2 inch) planar EDM flaw was strain gaged. Then alternating-load blocks of large and small amplitude load cycles were applied to mark the position of the crack front as it grew. During the test, strain surveys were made at the end of each loading block. In this way, the crack size and shape could be related to the local stress state as load was shifted due to crack growth. The measurements of crack shape and size were used as a check on the accuracy of crack growth predictions. The measurements of the local stress state were made because it was anticipated that they would be needed to put together a suitable stress intensity factor solution.

RESULTS

Raw Fatigue Test Data

Flat plate experiments. Table 7 lists the results from tests on the flat plate specimens. Figure 12a and 12b are S-N plots showing the results of all of the flat plate specimens with planar flaws tested at $R = 0.01$. Results of the tests run at $R = 0.01, 0.4$ and 0.6 are plotted in Figure 13. Note the apparent effect of mean stress in Figure 13a and the consolidation of this effect using $S_{mx}[(3-R)(1-R)/2]^{\frac{1}{2}}$ [1] in Figure 13b. This parametric expression serves as the basis to collapse data for various stress ratios onto a single resistance curve. Figure 14 compares data from volumetric flaw tests with data from planar flaw tests. (Note that the volumetric defect specimens failed at the backup ring. Because these specimens failed away from the volumetric defect, the true behavior of a volumetric defect cannot be isolated.)

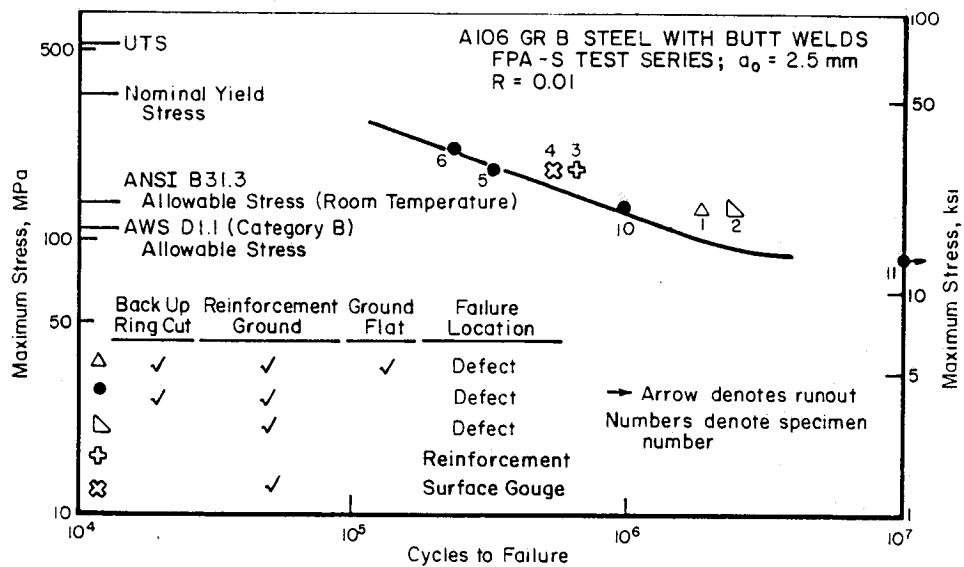
Pipe wall segment experiments. Table 7 also summarizes the data from the pipe-wall-segment specimens. Figure 15a shows a plot of these results. The pipe-wall-segment test results for artificial flaws of $a_0 = 5.1$ mm (0.2 inch) show only a slight decrease in life as compared to results of flat plate tests with the same size of artificial flaw. Data for wall segments with artificial and natural flaws are compared in Figure 15b. These results show that, for comparable defect sizes, artificial EDM defects are more severe than are natural defects as simulated in this study.

TABLE 7. RESULTS DEVELOPED USING FLAT PLATE AND WALL SEGMENT SPECIMENS

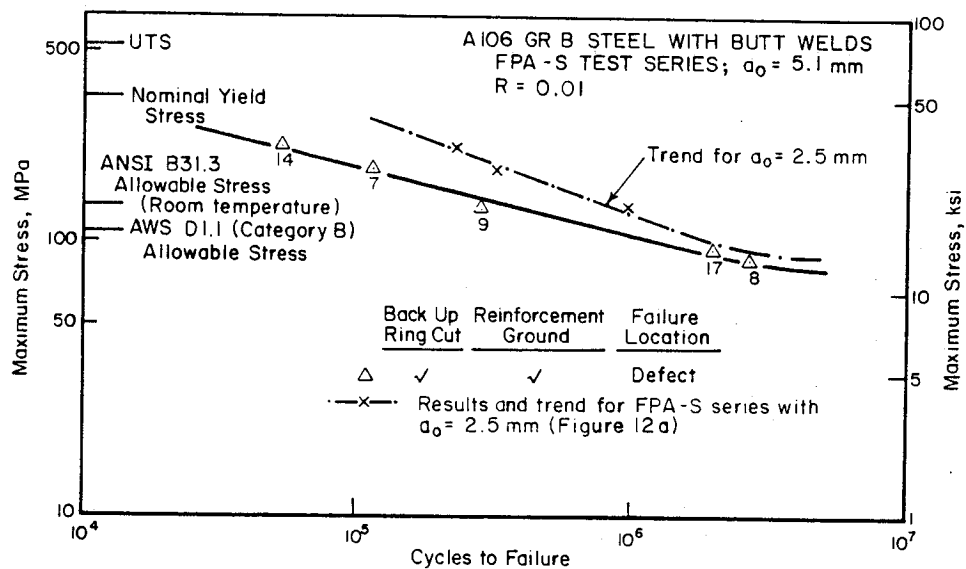
Specimen Number	Flaw Description		Semilength mm inch	R	Freq. (Hz)	S _{max}		Nf kilocycles	Comments		
	Depth mm inch					MPa	Ksi				
Center - Cracked Panel Specimen, EDM Through-Crack											
FPA-T-1	-	-	3.8	0.15	0.01	33	Varied	--	Reference Test		
Flat Plates, Artificial EDM Semi-Elliptical Surface Flaws											
FPA-S-1	2.5	0.1	3.8	0.15	0.01	33	91.0	13.2	2234.9	Surface ground backup ring intact, crack pinned by backup ring backup ring intact, fracture at weld toe backup ring intact, reinf. ground but failed away from EDM	
FPA-S-2	2.5	0.1	3.8	0.15	0.01	33	137.8	20.0	2414.7		
FPA-S-3	2.5	0.1	3.8	0.15	0.01	33	189.5	27.5	659.6		
FPA-S-4	2.5	0.1	3.8	0.15	0.01	32	189.5	27.5	541.7		
FPA-S-5	2.5	0.1	3.8	0.15	0.01	32	189.5	27.5	326.3		
FPA-S-6	2.5	0.1	3.8	0.15	0.01	10	227.4	33.0	234.8	Runout	
FPA-S-7	5.1	0.2	7.6	0.3	0.01	30	189.5	27.5	114.9		
FPA-S-8	5.1	0.2	7.6	0.3	0.01	20	137.8	20.0	2704.3		
FPA-S-9	5.1	0.2	7.6	0.3	0.01	20	137.8	20.0	287.8		
FPA-S-10	2.5	0.1	3.8	0.15	0.01	30	137.8	20.0	973.8		
FPA-S-11	2.5	0.1	3.8	0.15	0.01	30	89.6	13.0	10365.0		
FPA-S-12	2.5	0.1	3.8	0.15	0.6	30	275.6	40.0	1183.5		
FPA-S-13	2.5	0.1	3.8	0.15	0.6	30	316.9	46.0	711.0		
FPA-S-14	5.1	0.2	7.6	0.3	0.01	20	227.4	33.0	53.2		
FPA-S-15	2.5	0.1	3.8	0.15	0.4	20	316.9	46.0	141.3		
FPA-S-16	2.5	0.1	3.8	0.15	0.4	30	227.4	33.0	657.6		
FPA-S-17	5.1	0.2	7.6	0.3	0.01	20	96.5	14.0	1980.3		
FPA-S-18	2.5	0.1	3.8	0.15	0.4	20	189.5	27.5	1223.7		
Flat Plates, Artificial EDM Semi-Ellipsoidal Surface Flaws (Blind Holes)											
FPA-ES-1	2.5	0.1	3.8	0.15	0.01	20	227.4	33.0	313.9	Initiation away from EDM flaw	
FPA-ES-2	2.5	0.1	3.8	0.15	0.01	30	137.8	20.0	10400.0	Runout	
FPA-ES-3	2.5	0.1	7.6	0.30	0.01	30	189.5	27.5	484.3	Initiation at cut in backup ring	
FPA-ES-4	5.1	0.2	7.6	0.30	0.01	30	189.5	27.5	145.3	Initiation from backup ring	
Wall Segment Specimens, Artificial EDM Semi-Ellipsoidal Surface Flaws											
CPA-S-1	No flaw	-	-	-	-	-	-	-	-	Strain gaged specimen used to check bending Backup ring cut	
CPA-S-2	No flaw	-	-	-	0.01	20	227.4	33.0	145.9		
CPA-S-3	5.1	0.2	7.6	0.30	0.01	20	227.4	33.0	29.3	Cut in backup ring too deep Used to mark crack shape, growth	
CPA-S-4	5.1	0.2	7.6	0.30	0.01	20	137.8	20.0	257.1		
CPA-S-5	5.1	0.2	7.6	0.30	0.01	20	89.6	13.0	1814.8		
CPA-S-6	5.1	0.2	7.6	0.30	0.01	20	82.7	12.0	272.2		
CPA-S-7	5.1	0.2	7.6	0.30	0.01	20	172.3/89.6	25/13	--		
CPA-S-8	5.1	0.2	7.6	0.30	0.01	30	68.9	10.0	2439.5		
CPA-S-9	5.1	0.2	7.6	0.30	0.01	30	60.29	8.75	20500.0		
Wall Segment Specimens, Natural Welding-Induced Flaws											
CPN-1					0.01	20	189.5	27.5	100.4		Planar
CPN-2					0.01	20	189.5	27.5	2115.6		Volumetric
CPN-3					0.01	20	137.8	20.0	845.1	Planar	
CPN-4		intended size			0.01	10	227.4	33.0	54.6	Volumetric	
CPN-5		30.5 mm (1.2 in.)			0.01	20	189.5	27.5	334.1	Volumetric	
CPN-6		long 20 percent of wall			0.01	10	227.4	33.0	54.1	Planar	
CPN-7		thickness			0.01	15	227.4	33.0	157.8	Volumetric	
CPN-8					0.01	20	89.6	13.0	7228.0	Planar, runout defect not verified	
CPN-9					0.01	30	103.4	15.0	28.8	massive defect	
CPN-10					0.01	20	155.0	22.5	564.4	Volumetric	

ORIGINAL PAGE IS
OF POOR QUALITY

ORIGINAL PAGE IS
OF POOR QUALITY

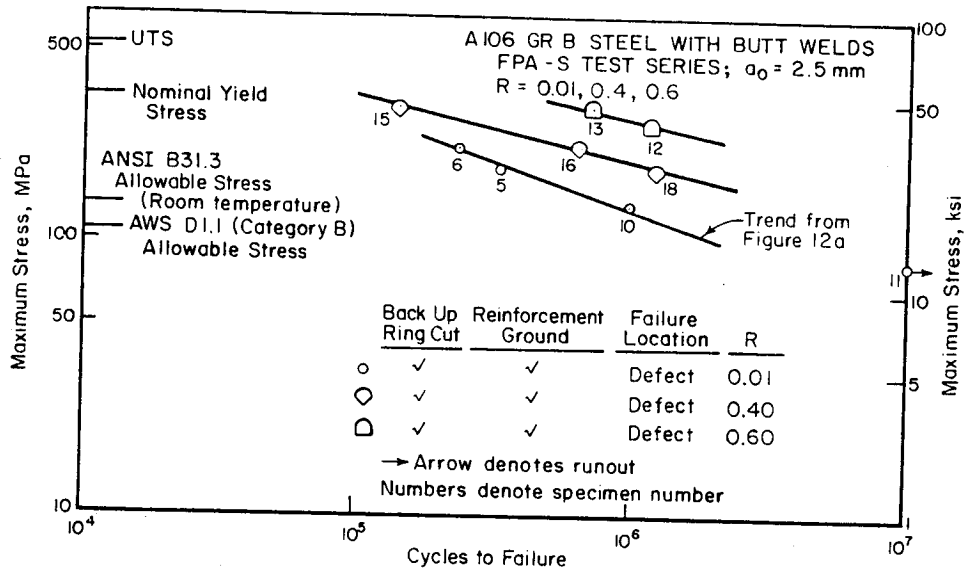


a. Initial flaw size of 2.5 mm (0.1 inch)

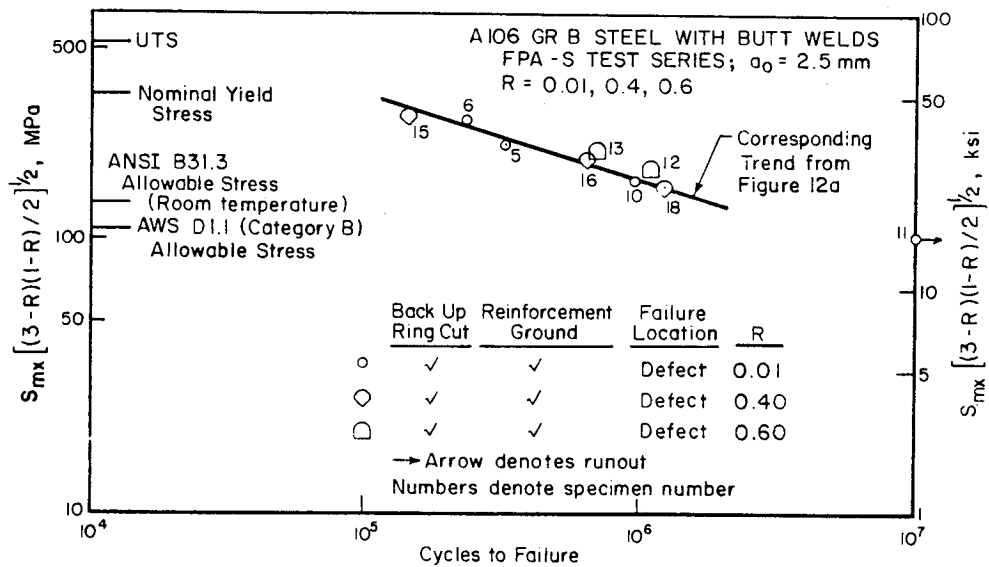


b. Initial flaw size of 5.1 mm (0.2 inch)

FIGURE 12. STRESS-LIFE BEHAVIOR OF FLAT PLATE BUTT WELD SPECIMENS WITH ARTIFICIAL PLANAR FLAWS (FPA-S)



a. On maximum stress versus life coordinates



b. Consolidated data using $S_{\max} [(3-R)(1-R)/2]^{1/2} [1]$

FIGURE 13. EFFECT OF MEAN STRESS LIFE BEHAVIOR OF FLAT PLATE BUTT WELD SPECIMENS WITH ARTIFICIAL PLANAR FLAWS (FPA-S)

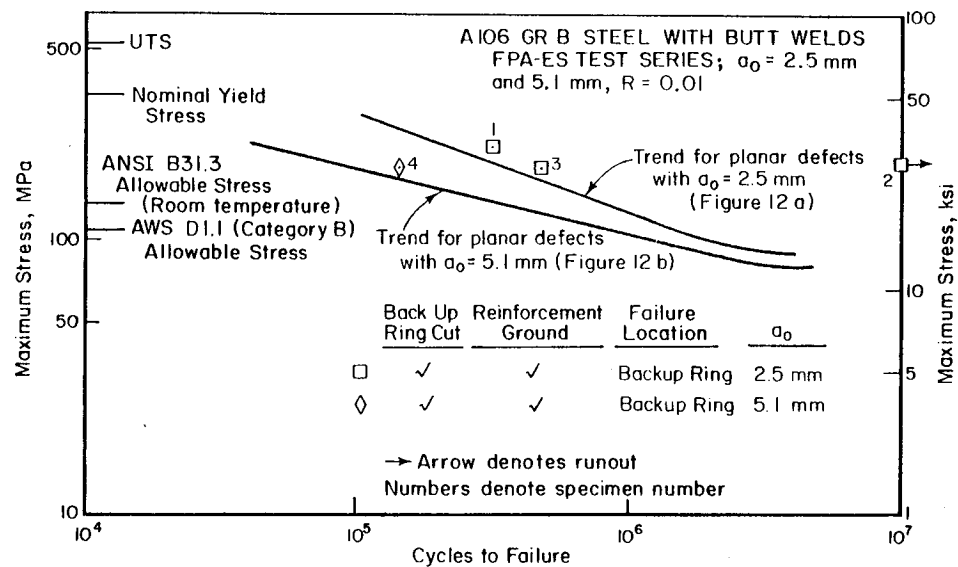
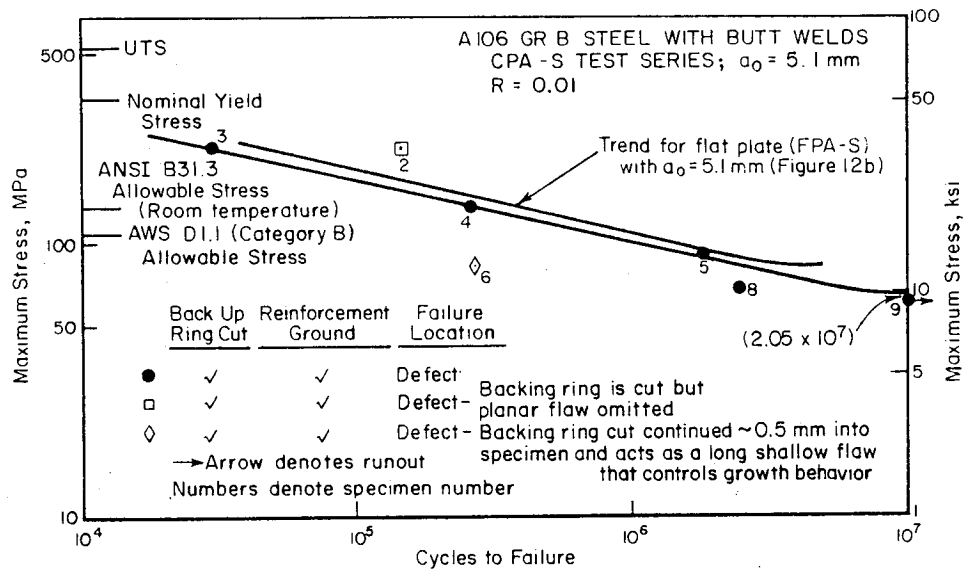


FIGURE 14. STRESS LIFE BEHAVIOR FOR FLAT PLATE BUTT WELD VOLUMETRIC DEFECT SPECIMENS (FPA-ES) IN COMPARISON TO PLANAR DEFECT SPECIMENS (FPA-S)

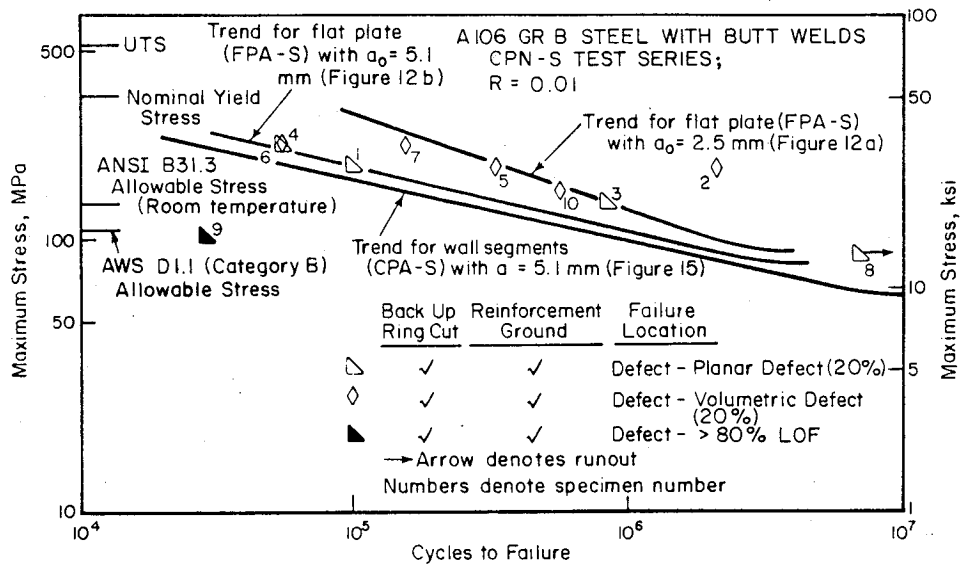
Pipe-segment experiments. Table 8 presents the data developed using the pipe-segment specimens. A total of 14 pipe-segment specimens were tested; twelve 203 mm (8-inch) diameter specimens and two 76 mm (3-inch) diameter specimens. Results for the 203 mm (8-inch) diameter specimens are broken down into three groups with four experiments in each group.

The first group of specimens contained artificial planar defects. Each of the failures for this group occurred in the artificially flawed center girth weld. The number of cycles to failure ranged from 377,360 cycles for the low axial stress case (52.9 MPa [7.7 ksi]) to 43,750 cycles for the high axial stress case (88.6 MPa [12.9 ksi]).

ORIGINAL PAGE IS
OF POOR QUALITY



a. Results for artificial defects with $a_0 = 5.1$ mm



b. Results for natural defects with $a_0 \sim 40$ percent by area

FIGURE 15. STRESS LIFE BEHAVIOR FOR BUTT WELDED WALL SEGMENT SPECIMENS (CPA-S)

TABLE 8. RESULTS OF PRESSURE CYCLING EXPERIMENTS FOR PIPE-SEGMENT SPECIMENS (a)

Specimen Number	Type of Flaw	Initial Flaw Size (b)				Max. Pressure MPa (psi)	Min. Pressure MPa (psi)	Axial Stress, MPa (ksi) (c)				Location of Failure	Number of Cycles at Failure
		Depth mm (inch)	Length mm (inch)					Max.	Range				
43Q1	Artificial Planar	4.95 (0.195)	213 (8.4)			13.7 (2000)	1.37 (200)	88.6 (12.9)	79.7 (11.6)			Center Girth Weld (d)	48,750
43Q2	Artificial Planar	4.95 (0.195)	213 (8.4)			11.0 (1600)	1.10 (160)	70.8 (10.3)	63.9 (9.3)			Center Girth Weld (d)	222,560
43Q3	Artificial Planar	4.95 (0.195)	213 (8.4)			9.6 (1400)	0.96 (140)	61.8 (9.0)	55.6 (8.1)			Center Girth Weld (d)	207,040
43Q4	Artificial Planar	4.95 (0.195)	213 (8.4)			13.7 (1200)	1.37 (120)	52.9 (7.7)	47.4 (6.9)			Center Girth Weld (d)	377,360
43Q5	Artificial Volumetric	4.95 (0.195)	213 (8.4)			13.7 (2000)	1.37 (200)	88.5 (12.9)	75.7 (11.6)			End Cap Weld (e)	48,000
43Q6	Artificial Volumetric	4.95 (0.195)	213 (8.4)			12.4 (1800)	1.24 (180)	75.7 (11.6)	71.4 (10.4)			Center Girth Weld (f)	387,970
43Q7	Artificial Volumetric	4.95 (0.195)	213 (8.4)			15.5 (2250)	1.55 (225)	99.6 (14.5)	89.3 (13.0)			Center Girth Weld (f)	96,670
43Q8	Artificial Volumetric	4.95 (0.195)	213 (8.4)			13.7 (2000)	1.37 (200)	88.6 (12.9)	79.7 (11.6)			End Cap Weld (e)	59,060
54P1	Natural Planar	4.95 (0.195)	213 (8.4)			13.7 (2000)	1.37 (200)	88.6 (12.9)	79.7 (11.6)			End Cap Weld (e)	147,950/
54P2	Natural Planar	4.95 (0.195)	213 (8.4)			15.5 (2250)	1.55 (225)	99.6 (14.5)	89.3 (13.0)			End Cap Weld (e)	176,840(h)
54P3	Natural Planar	4.95 (0.195)	213 (8.4)			17.0 (2475)	1.70 (247)	110. (16.0)	98.9 (14.4)			End Cap Weld (e)	226,640
54P4	Natural Planar	4.95 (0.195)	213 (8.4)			12.4 (1800)	1.24 (180)	79.7 (11.6)	71.4 (10.4)			End Cap Weld (g)	122,530
													1,337,850
NL1	Actual In-Service	(i)	(i)			22.7 (3300)	2.27 (330)	85.9 (12.5)	76.9 (11.2)			Base Metal of Piping Tee	36,970
NL2	Actual In-Service	(i)	(i)			22.7 (3300)	2.27 (330)	85.9 (12.5)	76.9 (11.2)			Base Metal of Piping Tee	189,320

(a) Pipe segments pressure cycled with hydraulic oil at a frequency of 1 Hz. Pressure waveform was a sine wave.

(b) Nominal planned flaw sizes.

(c) Based on a mean radius: $\sigma = P d i / (4 t (1 + t / d i))$.

(d) Specimens failed at EDM defect in center of girth weld.

(e) Specimens failed in one of the end cap welds. Failures attributed to high residual stresses due to welding of nipples or plugs into heads after specimen has been normalized.

(f) Specimens failed at EDM defect in center girth weld after end cap welds had been locally stress relieved with a torch.

(g) Specimen failed at an end cap weld after end cap weld had been locally stress relieved with a torch.

(h) First specimen which failed at an end cap weld. Initial failure at 147,950 cycles. Tried to grind out weld crack and repair. Specimen failed a second time 28,890 cycles after repair (total cycle count 176,840 cycles). Stopped test.

(i) Unknown since samples removed from service.

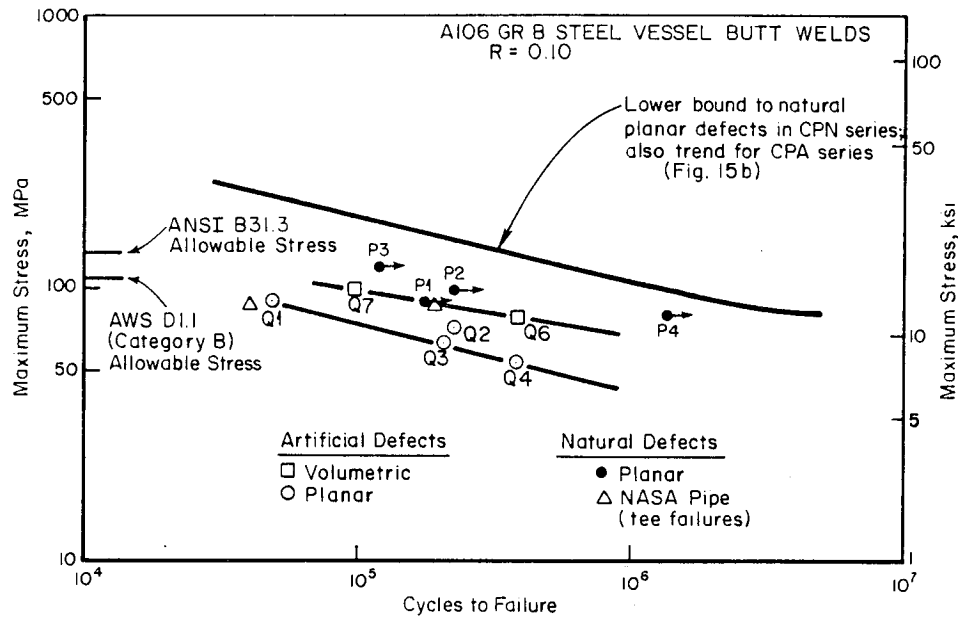
ORIGINAL PAGE IS
OF POOR QUALITY

The second group of 203 mm (8-inch) diameter specimens contained artificial volumetric defects. Two of the four specimens failed in the cap welds. These failures were attributed to high residual stresses. The maximum axial stress for both of these experiments was 88.6 MPa (12.9 ksi). One specimen experienced 48,000 cycles prior to failing at an end cap weld. The other experienced 59,060 cycles prior to failure. Post-test examination of the fracture surface for both of these specimens revealed no fatigue crack growth from the EDM notch. Valid failures occurred at 96,670 and 387,970 cycles for the other two specimens.

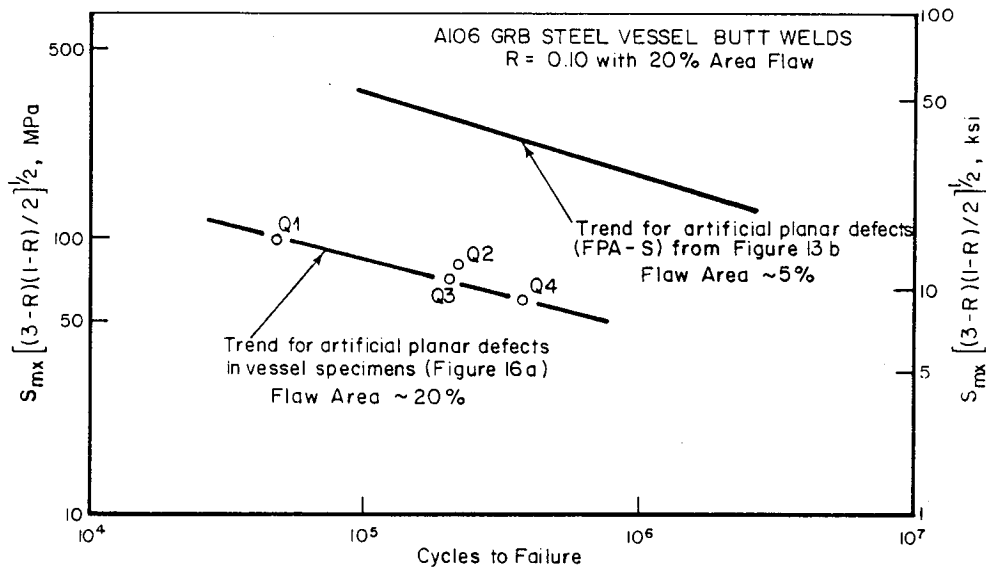
The third group of 203 mm (8-inch) diameter specimens contained natural planar defects. All four of these specimens failed in an end cap weld. Post-test examination of the fracture surfaces revealed that two of the four specimens had experienced some fatigue crack growth at the flawed centerline girth weld prior to failing at the end cap weld. The natural flaw for Specimen 54P2 had extended in depth approximately 1.3 mm (0.05-inch) for a length of approximately 33 mm (1.3 inches) after 226,640 cycles. The maximum axial stress for this experiment was 99.6 MPa (14.5 ksi). The natural flaw for Specimen 54P3 had extended in depth approximately 0.8 mm (0.03-inch) for a length of approximately 13 mm (0.5-inch) after 122,530 cycles. The maximum axial stress for this experiment was 110 MPa (16.0 ksi). The flaws for the two remaining specimens (54P1 and 54P4) had not extended after 176,840 and 1,337,850 cycles, respectively. The maximum axial stress for these two experiments was 88.6 MPa (12.9 ksi) for specimen 54P1 and 79.7 MPa (11.6 ksi) for Specimen 54P4.

Test results for failures initiating at the artificial flaws are plotted in Figure 16a. Results for planar flaws in vessels tested at $R = 0.1$ are compared to the trend for planar flaws with $a_0 = 2.5$ mm in flat plates at $R = 0.01$ in Figure 16b using the mean stress correlation demonstrated in Figure 13b. As plotted in Figure 16b, the mean stress parameter on the ordinate accounts for the differences in the mean stress for the vessel and wall segment test data shown in part a of this figure. Thus, the essential differences between the vessel and segment test data shown in Figure 16b are (1) flaw size and (2) biaxial and uniaxial stress states, respectively. Recall that the flaw size for the vessel test (about 20 percent area) was chosen to produce lives in the interval of interest to this program at reasonable pressures. Initial values of ΔK were nearly similar for the various geometries under these conditions. The results indicate that to get failure (a leak) in the vessels in a comparable number of cycles, an initial flaw size more than 4 times larger than for the flat plates ($a_0 = 2.5$ mm [0.1 inch]) is needed.

The two pipe-segment experiments were conducted on pipe samples removed from service. The maximum axial stress level for both of these specimens was 85.9 MPa (12.5 ksi). Results of these pipe tests are also plotted in Figure 16. Both specimens failed in the base metal of the pipe tee, well removed from any of the defective welds. The lives achieved by these specimens fall slightly below that for code rejectable planar defects (20 percent area) in vessel specimens. These tests indicate that code-unacceptable girth welds can have longer fatigue lives than unwelded portions of the piping system.



a. Stress-life behavior for planar and volumetric defects



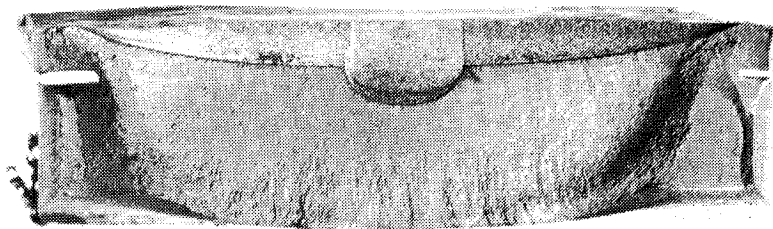
b. Comparison of planar defects for vessel and flat plate specimens

FIGURE 16. STRESS-LIFE BEHAVIOR FOR BUTT WELDED VESSEL TESTS LEADING TO FAILURE AT THE DESIRED DEFECT

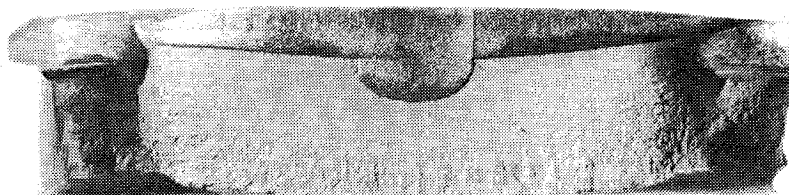
Fracture Surfaces

Fractography offers "after the fact" insight into the cracking process by study of the record left as the crack advanced. It also can be useful in assessing whether or not cracks sharpened or grew in otherwise unfailed specimens. Specimens were selected to either investigate the causes of aberrant data points or see if flaw sharpening or growth had occurred. When specimens had to be broken open, specimens were notched to locate the fracture plane as desired. Then the samples were fractured at near liquid nitrogen (LN_2) temperatures to reduce toughness and provide a distinct change in morphology. Lower power (3-30x) stereo optical microscopy was conducted to document failures. Supplementary higher power scanning microscopy was conducted to determine whether defects sharpened and grew somewhat in runout situations.

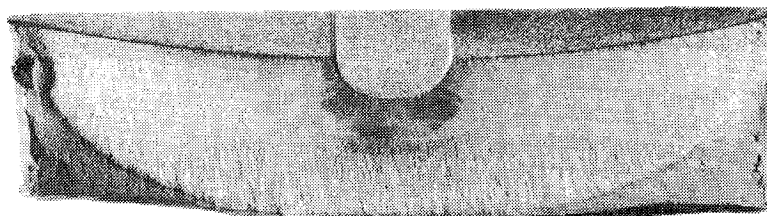
Flat plate specimens. Figure 17 shows the fracture surfaces of flat plate specimens with planar EDM flaws of depth $a = 2.5 \text{ mm}$ (0.1 inch) conducted at $R = 0.01$. The flaws of Specimen FPA-S-11, which was a runout, did not show evidence of growth, as illustrated by Figure 17d. (A deep saw cut was put in the specimen after testing to assist in breaking it open at liquid nitrogen (LN_2) temperature.) Pinning of the crack by an uncut backup ring is seen in Figure 17e and 17f. Note that both of these flaws were from the same specimen. Specimens FPA-S-3 and FPA-S-4 shown in Figures 17g and 17h both



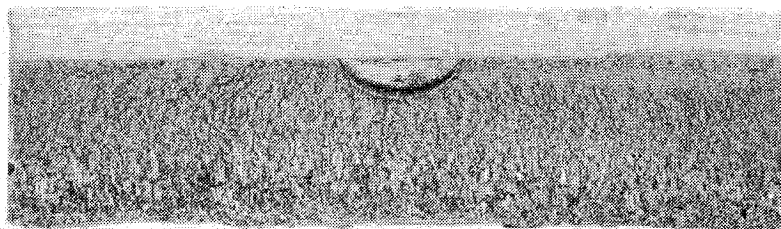
a. FPA-S-6 (8L484)



b. FPA-S-5 (8L472)



c. FPA-S-10 (8L482)

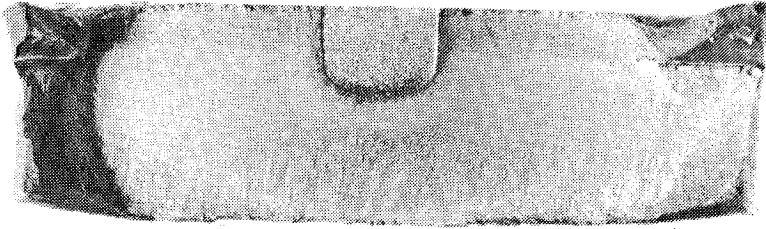


d. FPA-S-11 (IM457)

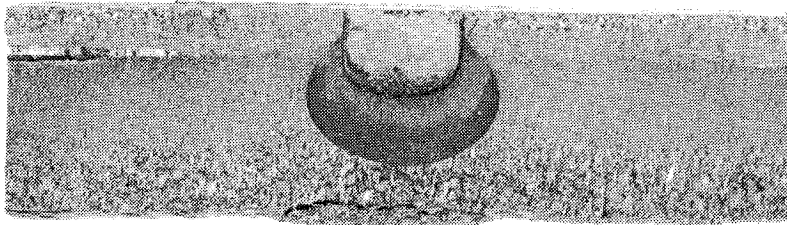
FIGURE 17. MACROGRAPHS OF FLAT PLATE SPECIMENS WITH
PLANAR FLAWS

Note: $a = 2.5 \text{ mm (0.1 inch)}$, $R = 0.01$
at 2X magnification

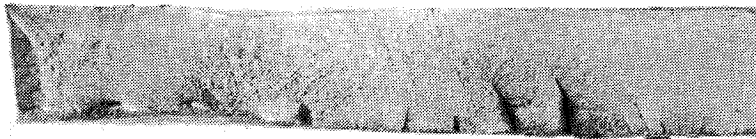
ORIGINAL PAGE IS
OF POOR QUALITY



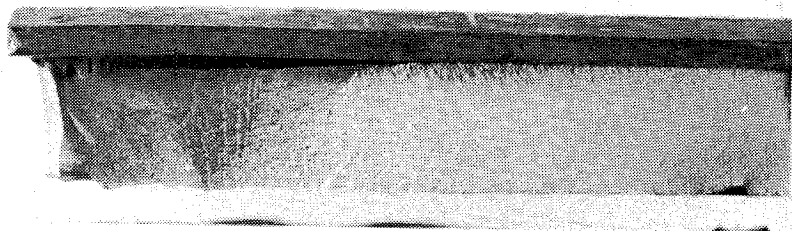
e. FPA-S-2 (8L478)



f. FPA-S-2 (8L503)



g. FPA-S-3 (8L503)



h. FPA-S-4 (8L481)

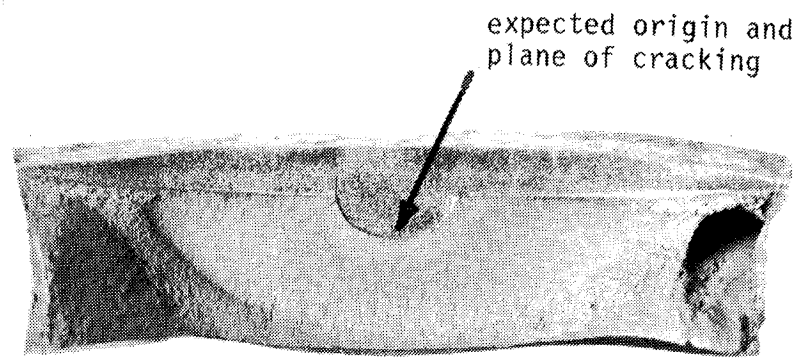
FIGURE 17. (Concluded)

failed at the weld toe. The weld toe was not ground on FPA-S-3. FPA-S-4 was ground, but the deep gouge near the corner caused the failure.

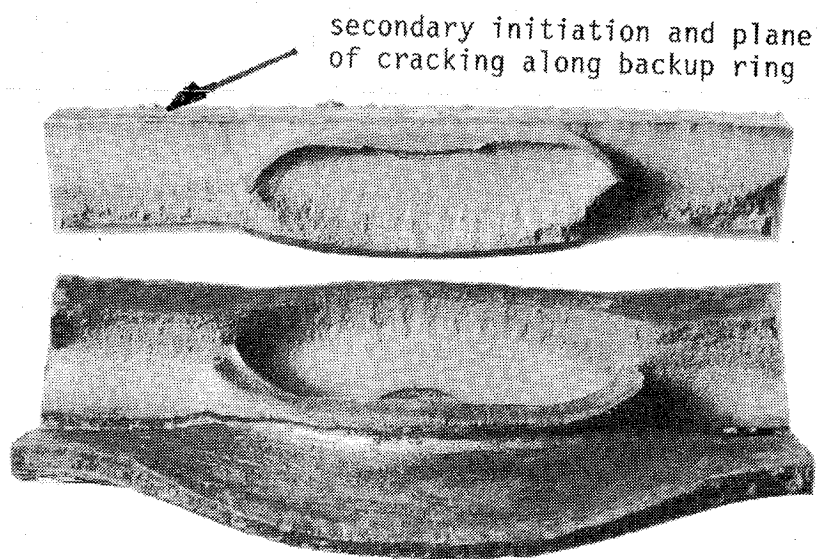
Macrographs for the flat plate specimens tested at $R = 0.4$ and 0.6 are shown in Figure 18. Except for the first specimen, fractures developed in two planes. One is the plane of the flaw, the other is the plane of one of the root faces in the base metal. These welds were supposed to be quality welds; however, NDI was not done for FPA-S-16 and FPA-S-18, and so the slight LOP was not detected. FPA-S-12 and FPA-S-13 passed NDI as quality welds.

Figure 19 presents macrographs for flat plate specimens with large planar flaws; $a = 5.1$ mm (0.2 inch). Fracture surfaces for specimens with EDM volumetric flaws are shown in Figure 20. Figure 20a illustrates that Specimen FPA-ES-1 failed as a crack grew from the backup ring. The crack plane intersected the EDM flaw. Figure 20c shows that the flaws of FPA-ES-2, a runout, did not sharpen. FPA-ES-4 is seen in Figure 20d to have failed due to a crack growing from the backup ring rather than from sharpening and growth from the EDM flaw.

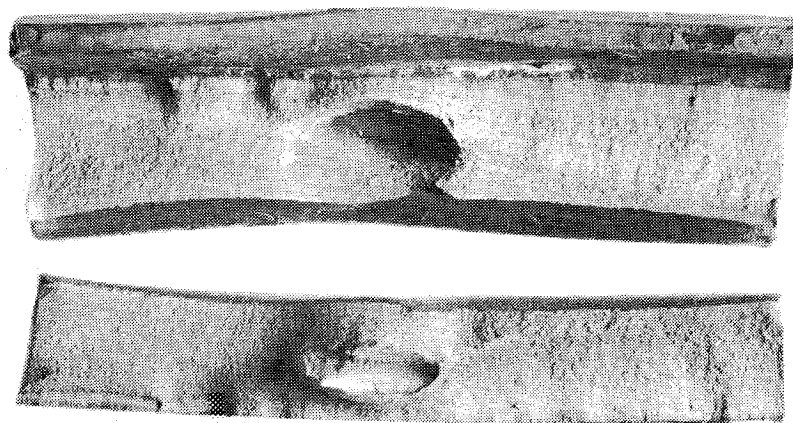
Pipe wall segment specimens. Figure 21 presents macrographs for pipe wall specimens with artificial flaws. The flaw of CPA-S-9 did not grow, as seen in Figure 21e. CPA-S-7 (Figure 21f) was marked by interspersing blocks of high and low amplitude loads. The marker bands cannot be seen at this magnification, nor could all of them be conclusively located at up to 2,500X magnification. Specimen CPA-S-2 is shown in Figure 21g. This specimen was inadvertently tested with no EDM flaw, but the backup ring was cut.



a. FPA-S-13 (8L480)



b. FPA-S-12 (8L470)

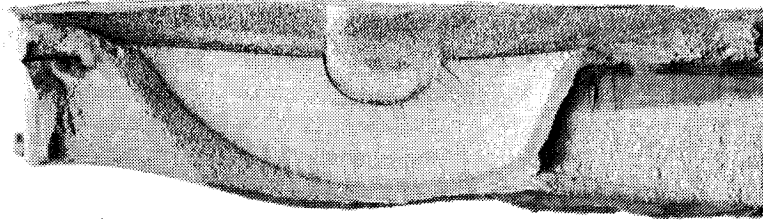


c. FPA-S-15 (8L473)

FIGURE 18. MACROGRAPHS OF FLAT PLATE SPECIMENS WITH PLANAR FLAWS

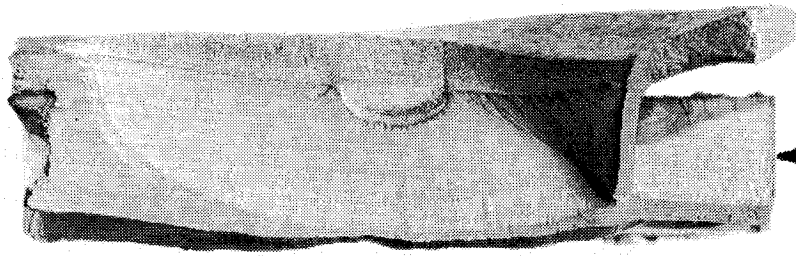
Note: $a = 2.5 \text{ mm (0.1 inch)}$, $R = 0.4, 0.6$

ORIGINAL PAGE IS
OF POOR QUALITY



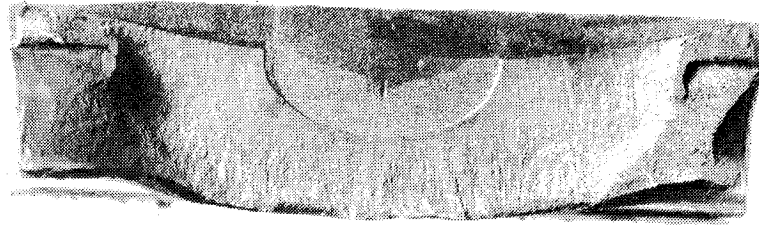
d. FPA-S-16 (8L485)

cracking from backup ring

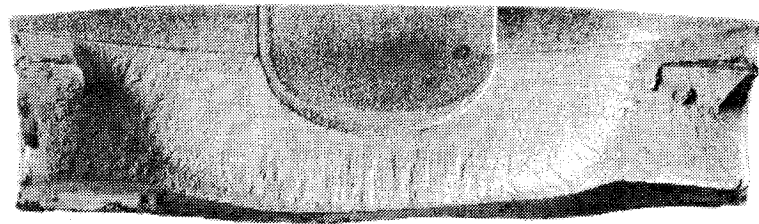


e. FPA-S-18 (8L487)

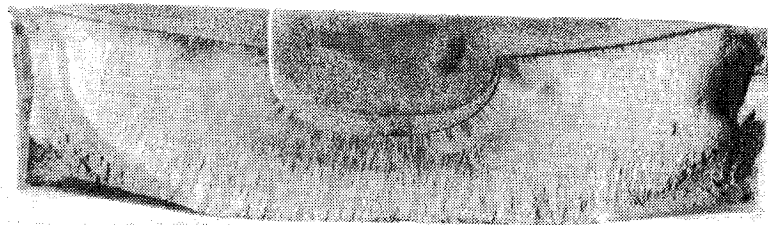
FIGURE 18. (Concluded)



a. FPA-S-7 (8L477)



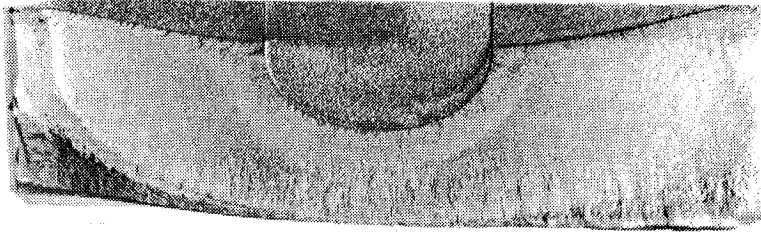
b. FPA-S-14 (8L474)



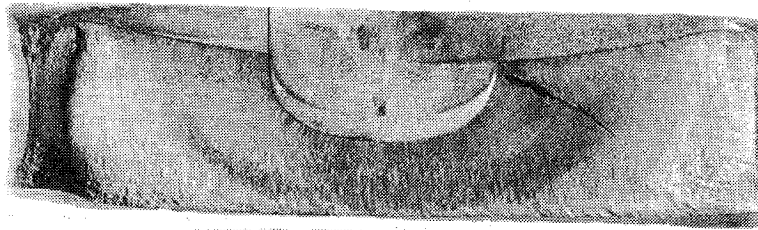
c. FPA-S-9 (8L479)

FIGURE 19. MACROGRAPHS OF FLAT PLATE SPECIMENS WITH PLANAR FLAWS
Note: $a = 5.1 \text{ mm (0.2 inch)}$

ORIGINAL PAGE IS
OF POOR QUALITY

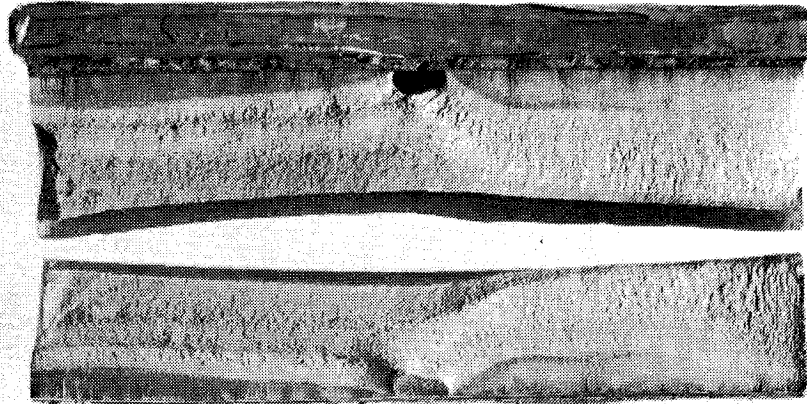


d. FPA-S-17 (8L486)

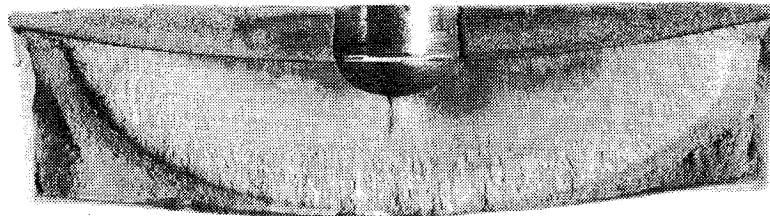


e. FPA-S-8 (8L475)

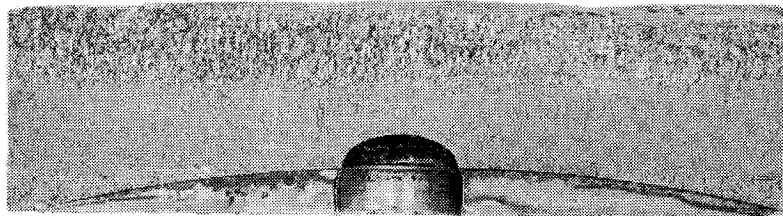
FIGURE 19. (Concluded)



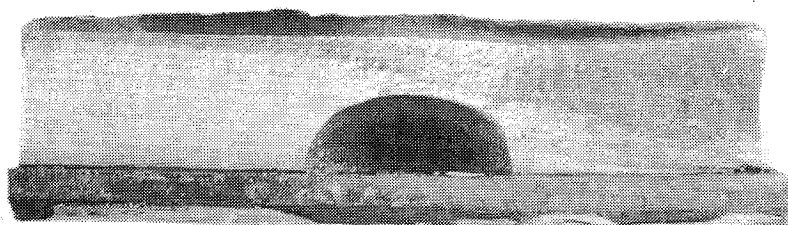
a. FPA-ES-1 (8L469)



b. FPA-ES-3 (8L483)



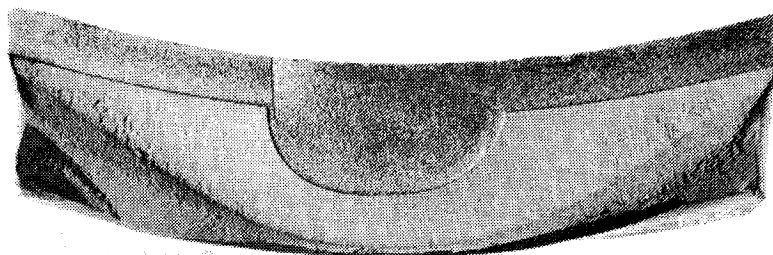
c. FPA-ES-2 (IM458)



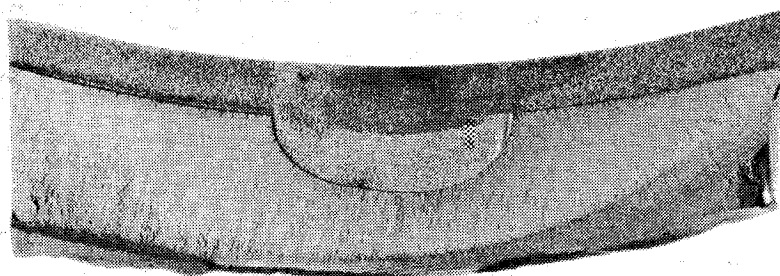
d. FPA-ES-4 (8L471)

FIGURE 20. MACROGRAPHS OF FLAT PLATE SPECIMENS WITH VOLUMETRIC FLAWS

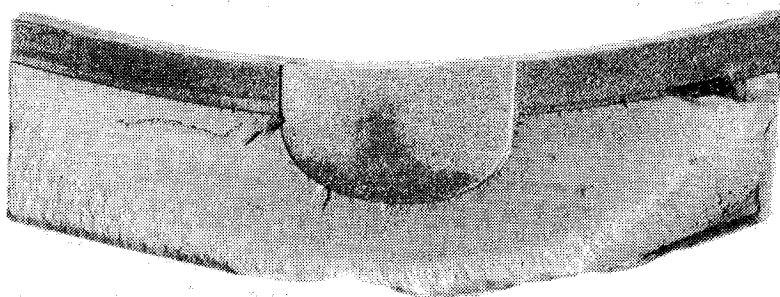
ORIGINAL PAGE IS
OF POOR QUALITY



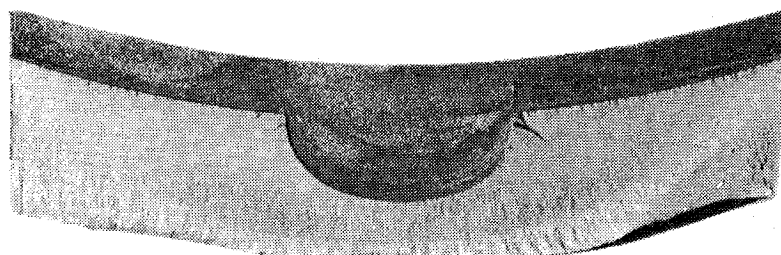
a. CPA-S-3 (8L490)



b. CPA-S-4 (8L488)

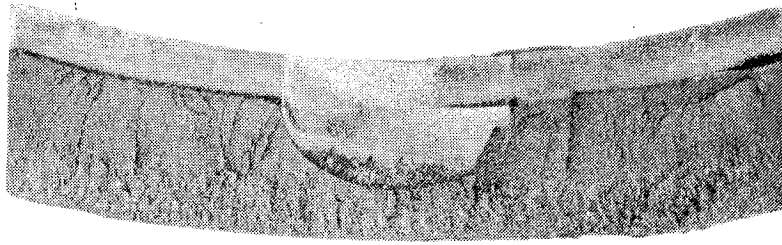


c. CPA-S-5 (8L492)

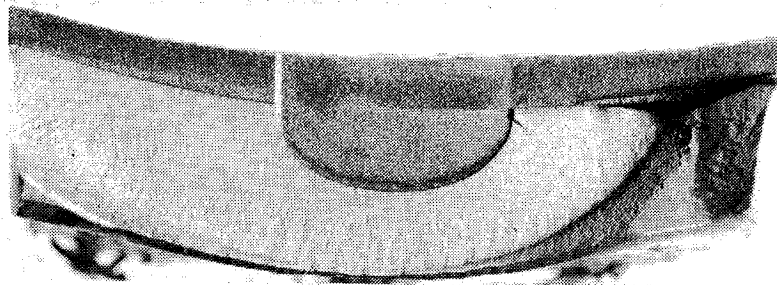


d. CPA-S-8 (8L491)

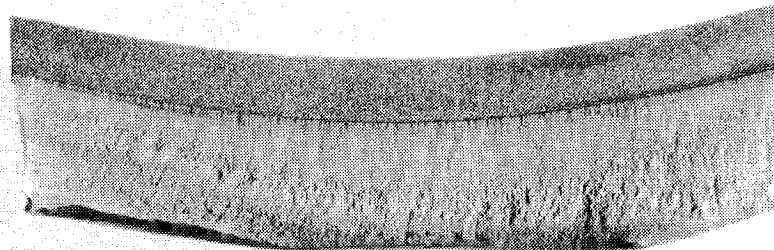
FIGURE 21. MACROGRAPHS OF PIPE WALL SPECIMENS WITH
ARTIFICIAL FLAWS



e. CPA-S-9 (IM459)



f. CPA-S-7 (8L502)

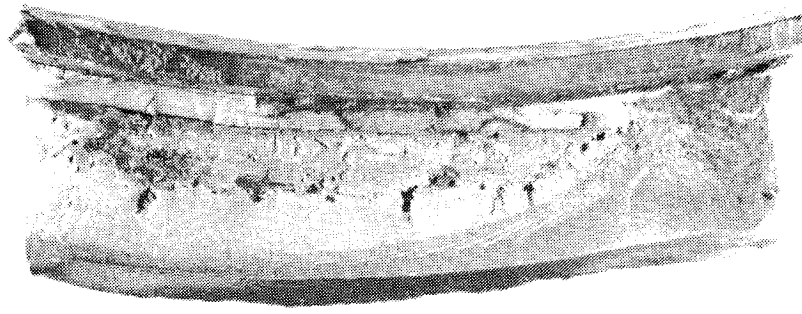


g. CPA-S-2 (8L489)

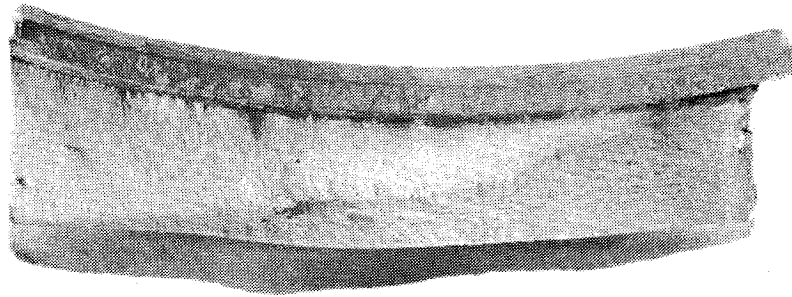
FIGURE 21. (Concluded)

Macrographs for pipe wall specimens intended to have volumetric natural defects are shown in Figure 22a through 22e. For those intended to have planar defects, macrographs are shown in Figure 22f through 22j. Note in Figures 22b and 22e that the desired porosity was not produced. Radiographs were not taken of these specimens (which would have revealed the problem.). Similarly, Specimen CPN-9 (Figure 22i) had massive LOP and porosity. This specimen was from the group of specimens which were not radiographed. Specimen CPN-8V, a runout, is not shown. Efforts to break it open at LN_2 temperature were unsuccessful.

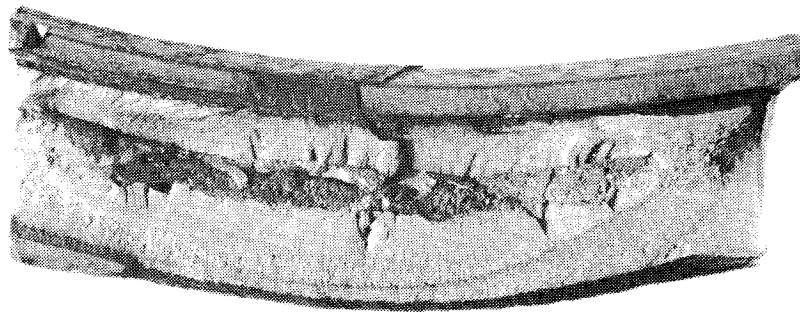
Vessel specimen. Figure 23a presents macrographs at the deepest penetration of the preflaw or in the region where the crack grew through the wall in Vessels 43Q1, 43Q2, 43Q5, and 43Q7. For Q1, Q2, and Q7, failure occurred by penetration of the crack in the area shown. However, for Q5 failure occurred at a "quality weld" at the end cap. Examination of the area at the root of the defect showed the crack had begun to grow at a number of sites along the root. Figure 23b presents ring sections of two vessels over which cracking occurred. Observed that for Specimen 43Q1 the defect extended into the wall primarily over its mid section, thereby decreasing the aspect ratio.



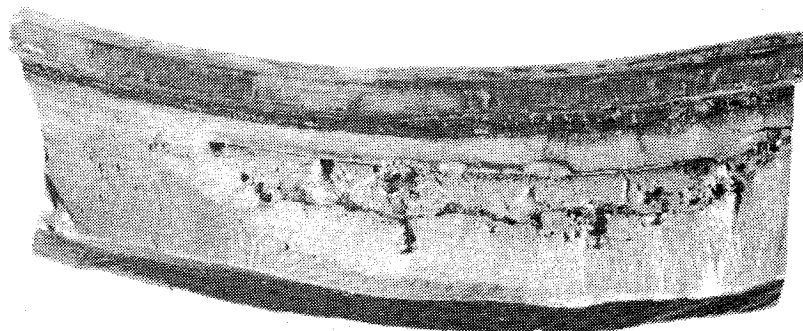
a. CPN-4V (8L495)



b. CPN-7V (8L499)



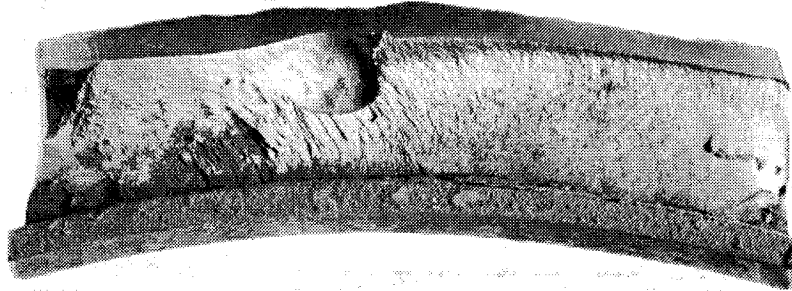
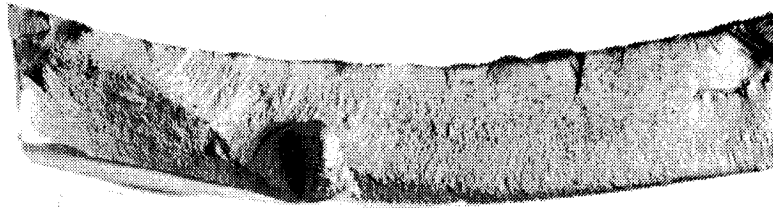
c. CPN-2V (8L494)



d. CPN-5V (8L497)

FIGURE 22. MACROGRAPHS OF PIPE WALL SPECIMENS WITH NATURAL VOLUMETRIC (V) AND PLANAR (P) FLAWS

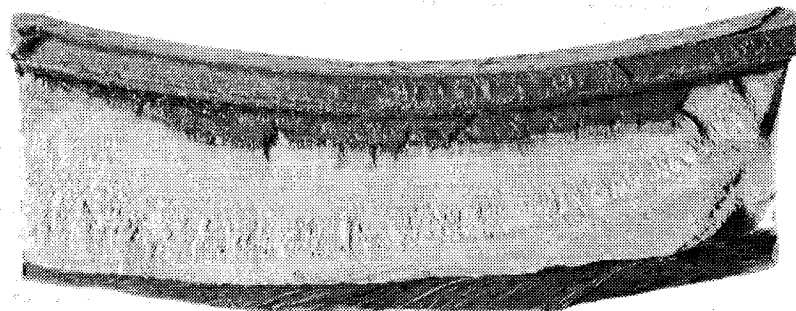
ORIGINAL PAGE IS
OF POOR QUALITY



e. CPN-10V (8L500)

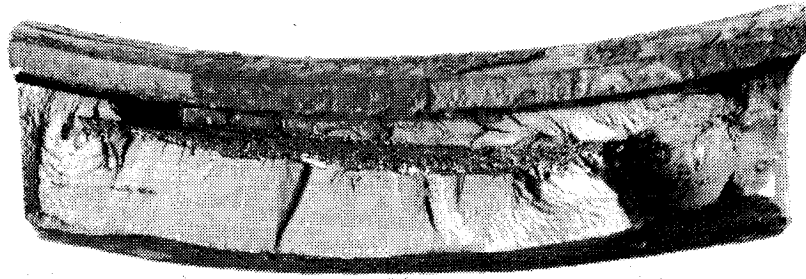


f. CPN-6P (8L498)

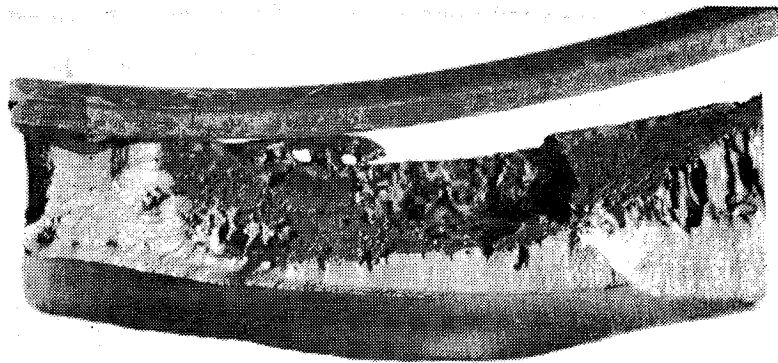


g. CPN-1P (8L493)

FIGURE 22. (Continued)



h. CPN-3P (8L496)

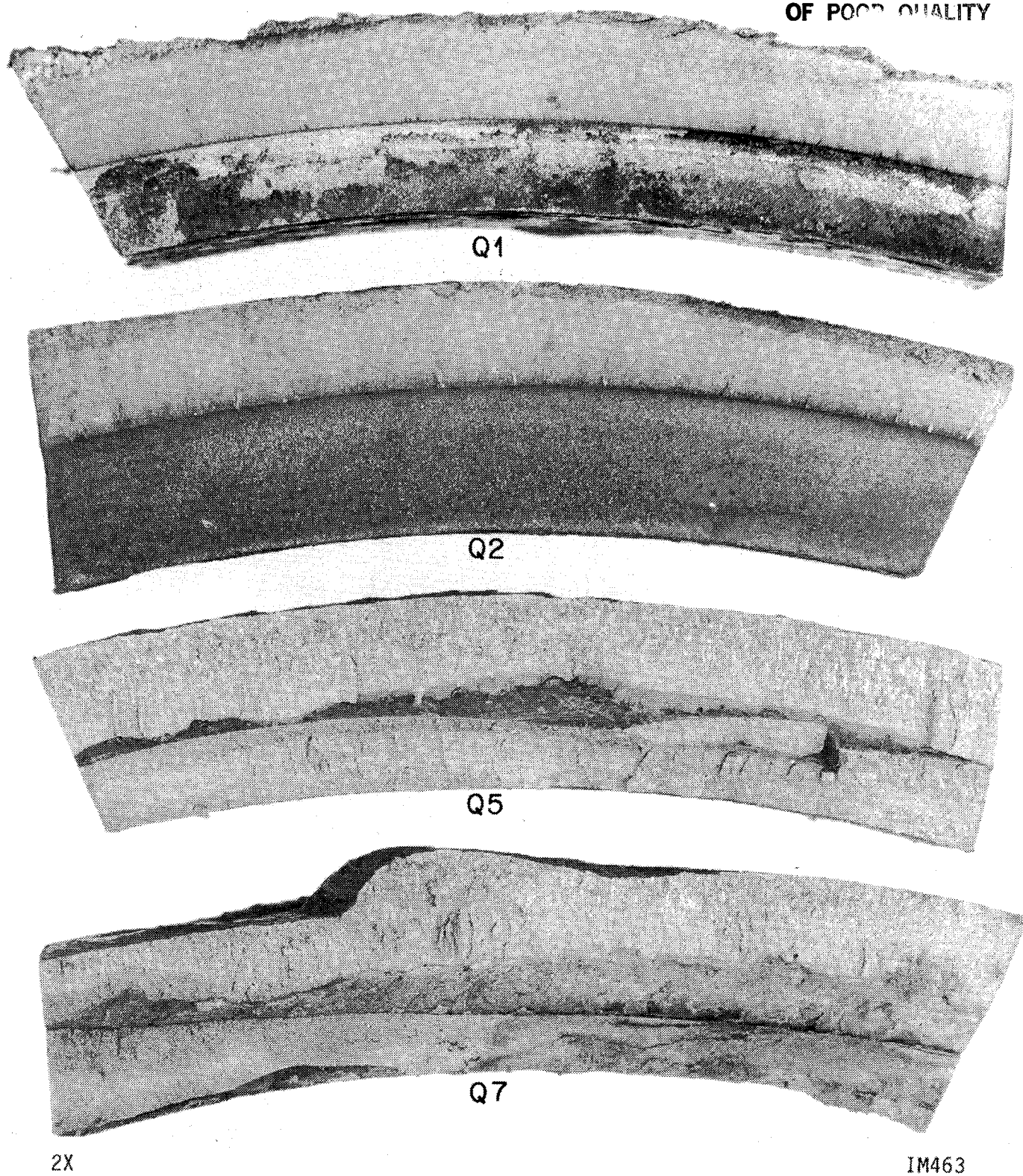


i. CPN-9P (8L501)

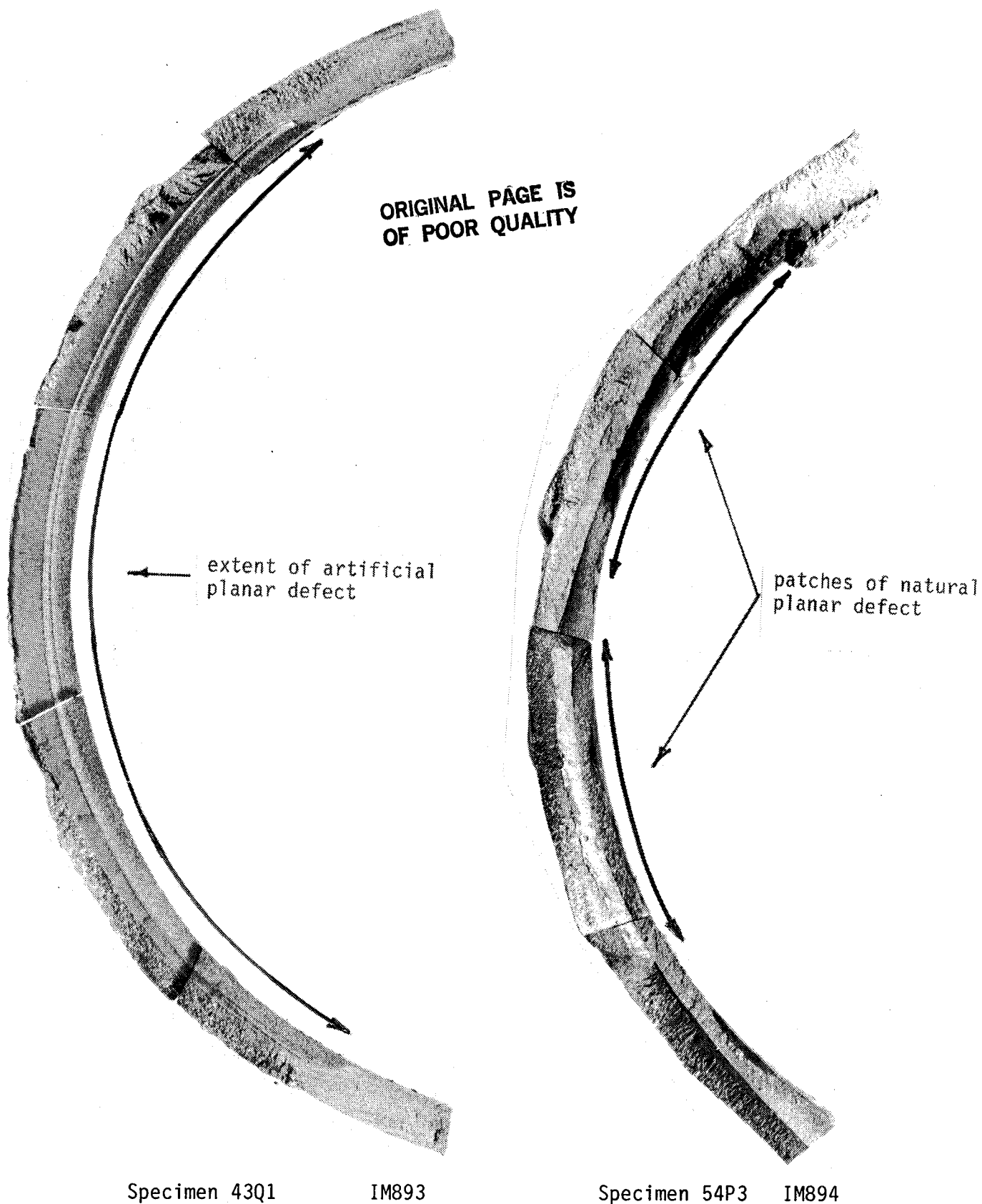
(No photograph available as the detect
could not be opened at flaw)

j. CPN-8P

FIGURE 22. (Concluded)



a. Views at segments containing the deepest penetration
FIGURE 23. MACROGRAPHS OF VESSEL SPECIMEN FRACTURE SURFACES



b. Ring Segments depicting extent of propagation around the vessel

FIGURE 23. (Concluded)

DISCUSSION

Viability of LEFM for Data Analysis and Interpolation

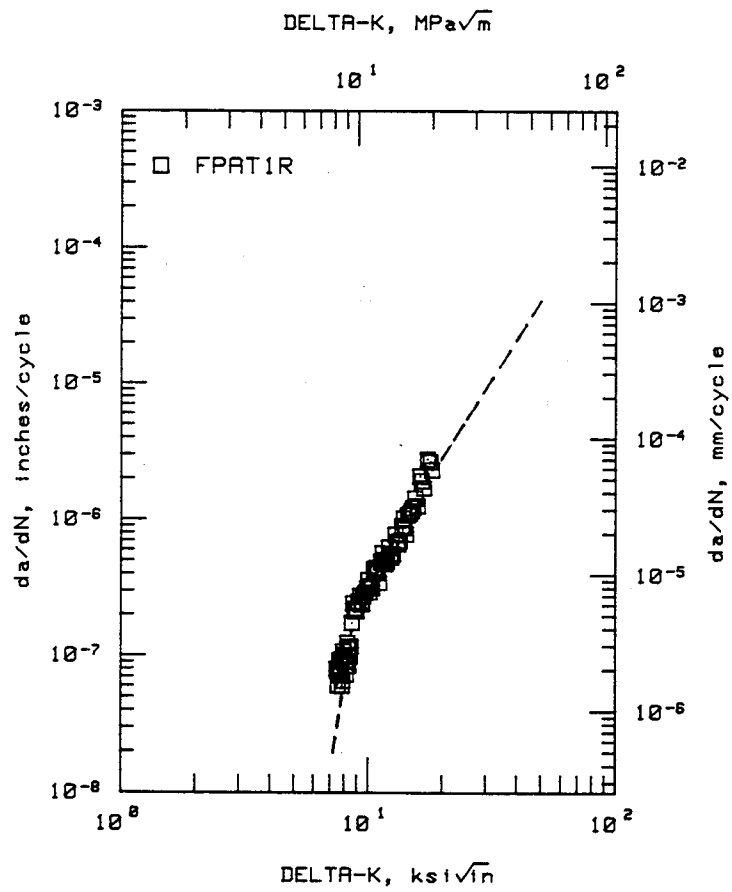
The ultimate objective of this study--to develop acceptance criteria for code rejectable indications--was to be met by supplementing the results of the literature search with a limited application specific data base. Raw data presented in the previous section provide this application specific database. This data base also was to serve as a benchmark database to calibrate a LEFM based life prediction capability for defects in piping. In turn, this life prediction capability was to be used to develop defect acceptance criteria for A106 Gr. B piping. These criteria were to cover a variety of defect shapes and sizes, pressures, diameters and wall thicknesses. Clearly, the relevance of LEFM to the problem at hand must be shown before proceeding with LEFM-based criteria development.

The ability of the LEFM technology to predict observed behavior and correlate observed trends will be used as the basis to assess relevance. If LEFM calculations correlate the data or produce life-predictions which compare reasonably with the observed behavior, LEFM then could be used as a tool to interpolate between and extrapolate beyond the experimental results. This would generate a data base of S-N curves for geometries with defect shapes and sizes other than those tested. Likewise LEFM could be used to develop defect acceptance criteria for weldments in piping systems. Each of the elements of a LEFM life prediction capability is explored for the problem at hand in the ensuing paragraphs.

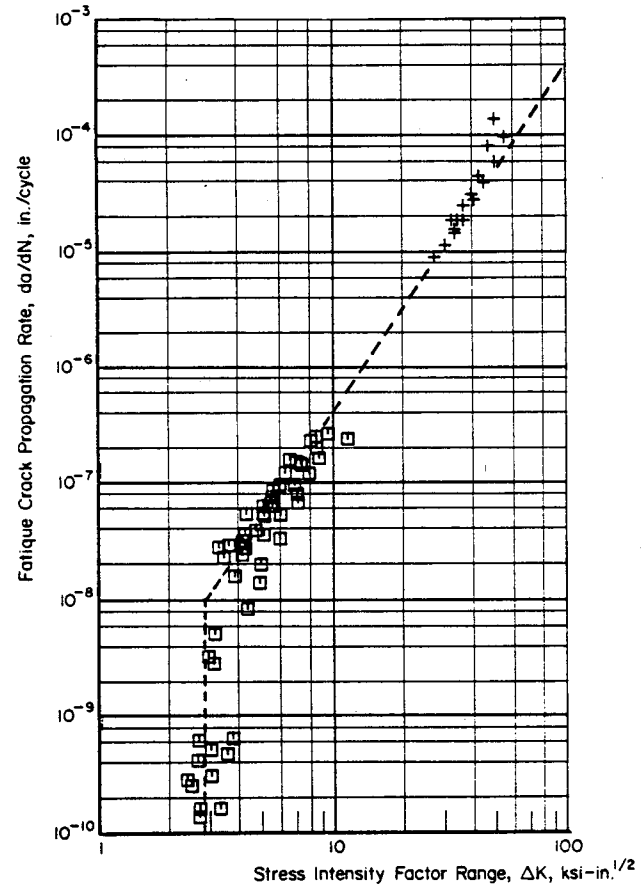
LEFM crack growth predictions require a proper description of the $\frac{da}{dn}$ versus ΔK data for the material at the stress ratio of interest. Such data have been developed in a reference test using a specimen with a through crack in the weld (Specimen FPA-T-1). The data developed in the reference test are shown in Figure 24a. These data follow a trend like that shown in Figure 24b†, which reproduces literature data for A106 GR B [4,5] base metal. Comparing the data in parts a and b of Figure 24 shows that the early crack growth rate results for the reference test fall below the literature trend. The reason for this is that there is a start-up transient in fatigue crack growth rate tests. A start-up transient is the period of time for some flaw--natural or artificial--to develop into a sharp crack with an established wake of plasticity. Such transients are not present in the literature data. This is because test standards like ASTM E647 require that they be removed. However, these transients must be considered when predicting the fatigue lives of structures.

For present purposes, the equation deemed to best fit the data was the equation which yielded acceptable predictions of the crack length versus cycles behavior for the growth rate data shown in Figure 24a. An interactive fatigue crack growth integration program has been used to make these trial and error calculations and all subsequent crack growth predictions. Figure 25 shows the results of a-N calculations for two trials. One trial used the log-log linear Paris equation. The other trial used a bilinear empirical equation, chosen to match the early growth rate $da/dN-\Delta K$ data. (The bilinear segments used are indicated in Figure 24a.)

† Note that near threshold trends for weld metal may differ from that of base metal because of differences in microstructure and crack closure.



a. Weld metal, this investigation



b. Base metal; after [4,5]

FIGURE 24. FATIGUE CRACK GROWTH RATE BEHAVIOR FOR A106-GRB

Observe in Figure 25 that excellent recreation of the a - N trend required the bilinear equation. This bilinear equation gave the correct a - N trend because it included the transient behavior that otherwise was ignored by the log-log linear fit.

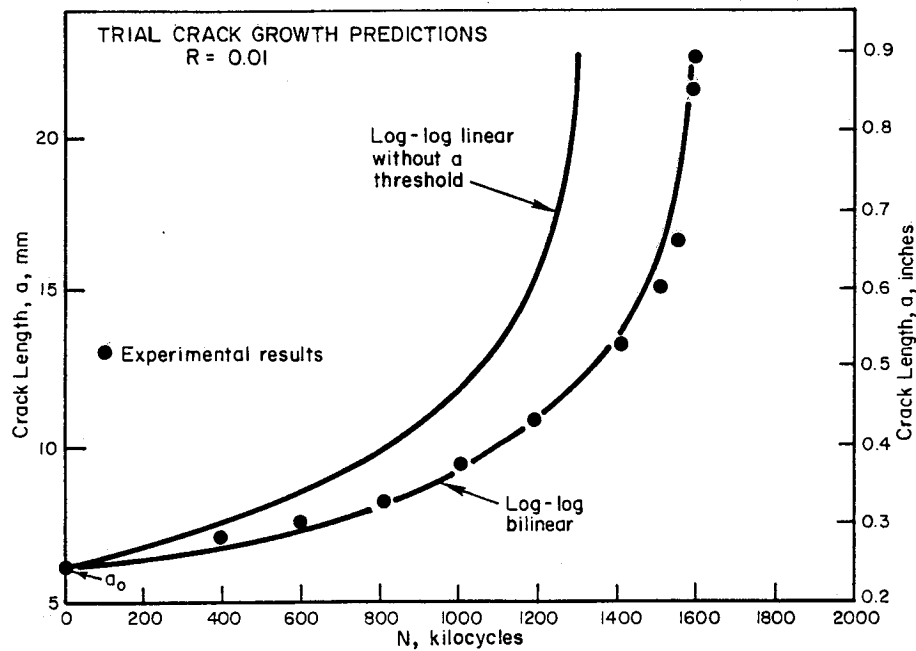


FIGURE 25. COMPARISON OF CRACK GROWTH RESULTS VS EXPERIMENT FOR TWO REPRESENTATIONS OF THE CRACK GROWTH CRACK RATE DATA

The linear fit with a threshold to match the data shown in Figure 24b is a better representation of steady state FCP behavior for the A106 GR B material. However, the bilinear equation better represents the growth process in the specimen since it accommodates the real startup transient. Differences between predictions made with a steady state trend for

an established crack and the actual behavior, including the transient period, will be accentuated in cases where the transient period dominates the life of the specimen (or structure). Factors that influence the transient period are the same as those controlling steady state growth. These factors include stress level, defect shape, defect size, i.e., defect type ("sharpness") and plasticity at the crack tip. Differences in the closure behavior at a sharpening defect as compared to a "steady state" crack may be a key to predicting the total life of welds containing defects.

Once a steady state crack develops, the resulting crack no longer remembers its origin--so defect type no longer is a factor. This can be seen by comparing a-N trends in Figure 25. For crack lengths longer than about 7.5 mm (0.3 inch), the result from the bilinear fit can be obtained by adding a constant number of cycles to the log-log linear result. This constant number of cycles can be interpreted as the "startup transient" portion of the life. For LEFM calculations to be useful in a practical predictive or correlative role, this startup transient would have to represent a small fraction of the total life. Alternatively, the transient period would have to be a "material" constant or a simple function of the specimen and defect geometry. (Stress level and crack size could be accounted for if their effect could be uncoupled and closure accounted for.)

It follows that the relevance of LEFM can be assessed by comparing predicted and observed lives, with a view to characterizing the startup transient. This must be done both for specimens and for the application of interest--piping.

The second element of an LEFM correlation and/or growth prediction capability is the stress-intensity factor for the geometry and flaw of interest. There are numerous equations in the literature for semi-elliptical surface cracks subjected to remote tension. In this study, the empirical stress-intensity factor of Newman and Raju [3] has been used. One attraction of this equation is that it can deal with both tension and bending loads. This makes it possible to examine the effect of specimen bending which was observed in pipe wall segment specimens. The equation for the stress intensity factor has been obtained by curve-fitting stress-intensity factors obtained from three-dimensional finite-element analyses. For discussion of the accuracy of the equation and comparison with experimental results, the reader is referred to Reference 3. Note that the K solution adopted does not include provision for stress concentration effects that might arise due to the backup ring. The backup ring could cause a significant localized gradient that varies longitudinally and through the thickness.

The third element of an LEFM correlation or crack growth rate prediction capability is an accurate estimate of the initial flaw size. For the present program, flaw size has been controlled during manufacture, verified by indirect measurements prior to testing, and, when feasible, accurately measured following failure. Initial flaw size, therefore, is accurately characterized, particularly for specimens used to assess the viability of LEFM. Artificial defects were developed in this study with EDM technology and "sharp" electrodes (cf Figure 3). The recast zone at the tip

of the defect exists in a steep thermal gradient, presumably creating a local tensile residual stress field that would promote sharpening of the defect into a crack. Thus, these sharp-defects have been assumed to be crack-like.

The crack-growth-integration computer program calculated the stress intensity factor at the deepest point of the crack, and at the crack tip at the surface. Crack growth was then determined at these points and the crack aspect ratio (depth/semi-length or a/c) was allowed to change. After the crack depth, a , became equal to the thickness, t , the program treated the crack as a through crack with an initial semi-length equal to the semi-length of the surface crack.

Note that LEFM calculations, based on Figure 24b, assume the defect is crack-like and that cracks will grow from the defect just as they would from a prior existing crack. That is, they do not account for a start-up transient. Accounting for start-up transients would require knowledge of the transition in growth rate behavior from defect through to a steady state crack. The more fatigue life spent in this transition, the worse the prediction. In an attempt to represent the startup transient for the present experimental program, the data of Figure 24a are taken as characteristic of the "crack sharpening" behavior of the material. Accordingly, the bilinear behavior evident in Figure 24a has been used to characterize the material, and used for all subsequent predictions. Such predictions tend toward an upper bound on total life in that they underestimate the growth rate for steady state FCP shown in Figure 24b. Spot comparison predictions for the corresponding case of no startup transient also have been made. These comparisons use the steady state FCP data trend in Figure 24b. In selected cases

these predictions ignore the existence of the threshold. Ignoring the threshold will predict a lower bound on the life as compared to the trends in Figure 24a and 24b. At higher initial stress intensities (those above the threshold), the log-log linear trend that ignores the threshold will lead to predictions similar to that for data fits to either trend in Figure 24. (In this respect, an empirically calibrated threshold could be used to force predictions to match observed life.)

Examination of the fracture surfaces and estimation of net section stresses at failure indicate that tensile failure of the net section caused specimen separation. Accordingly, a "net section" failure criterion was used to set the crack size at failure for specimens subjected to tension cycles. When the net section stress equalled the ultimate strength of the base metal, the specimen was considered to have failed.* This was done, recognizing that LEFM is invalid in such applications, so that the failure criterion would partially account for post-yield crack growth. It will be shown later that the conclusions drawn from the fracture mechanics study do not depend strongly on the failure criterion (since very little of the life is spent under net section yield conditions). Thus the choice of the failure criterion is really a moot point. It is not a factor for vessel tests since failure for those specimens is defined as a leak.

* The average measured ultimate strength of the base metal was 542 MPa (78.9 ksi); the specified minimum ultimate strength of the weld metal could have been used, in view of the relatively small difference, the choice of the former values makes little difference. Also, the total predicted life is affected only slightly by variations in the failure criterion.

The utility of fracture mechanics was first assessed via predictions of the fatigue lives of flat plate specimens. The specimen dimensions and stress levels were input to the computer program for specimens with planar EDM flaws. Predictions were made for specimens tested at $R = 0.01$. Figures 26 and 27 present the results of the life predictions.

Figure 26 compares predicted and observed fatigue lives for the small planar flaws ($a = 2.5 \text{ mm}$ [0.1 inch]). This figure shows the predictions account for only 26 to 35 percent of the actual lives. For the large flaws ($a = 5.1 \text{ mm}$ [0.2 inch]), Figure 27 shows that the predictions account for only 11 to 28 percent of the actual lives. Note that these underpredictions exist for the case of a simple test geometry and a simple flaw geometry with a known size. Note further, that the initial stress intensity is well above the threshold level. These predictions also represent results developed with a da/dN curve that includes the "startup transient" of the flat plate specimen. As such, they represent a lower bound as compared to the linear curve with a threshold that fits the data in Figure 24b.

Selected predictions made using Figure 26b show similar results for the higher stresses for both initial flaw sizes. At the lower stresses, predictions made with the linear trend in Figure 24b, with or without a threshold, lead to comparable results since initial K levels are in excess of the threshold. For all cases with $a_0 = 5.1 \text{ mm}$, the difference between the predictions made using Figures 24a and 24b is less than +1 percent. The same is true at higher stresses for $a_0 = 2.5 \text{ mm}$. However, at lower stresses, life predictions begin the integration at ranges of stress intensity factor that fall at or below the so called threshold in Figure 24b or in the start-up

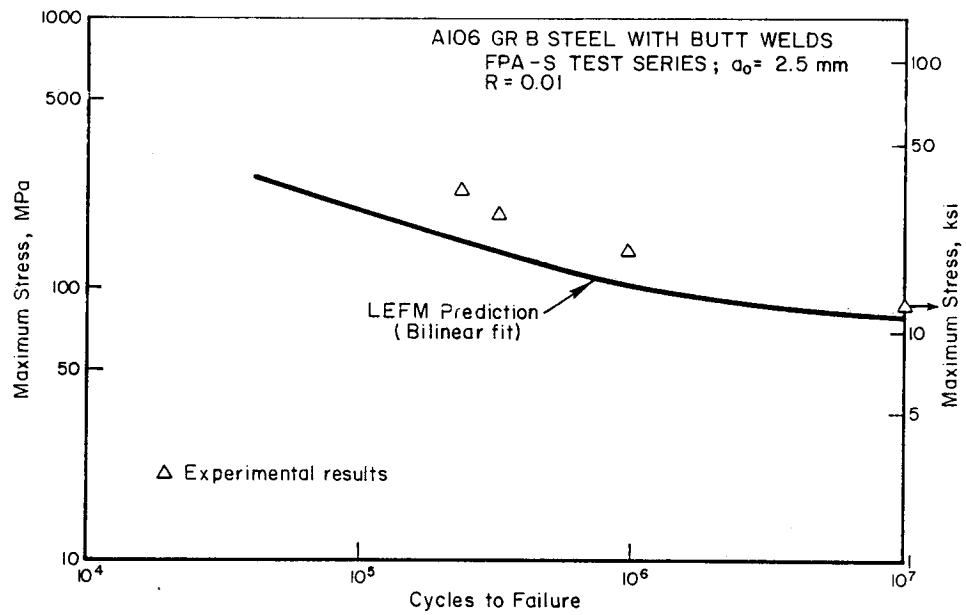


FIGURE 26. COMPARISON OF PREDICTED AND ACTUAL LIFE FOR FLAT PLATE SPECIMENS WITH $a_0 = 2.5$ MM

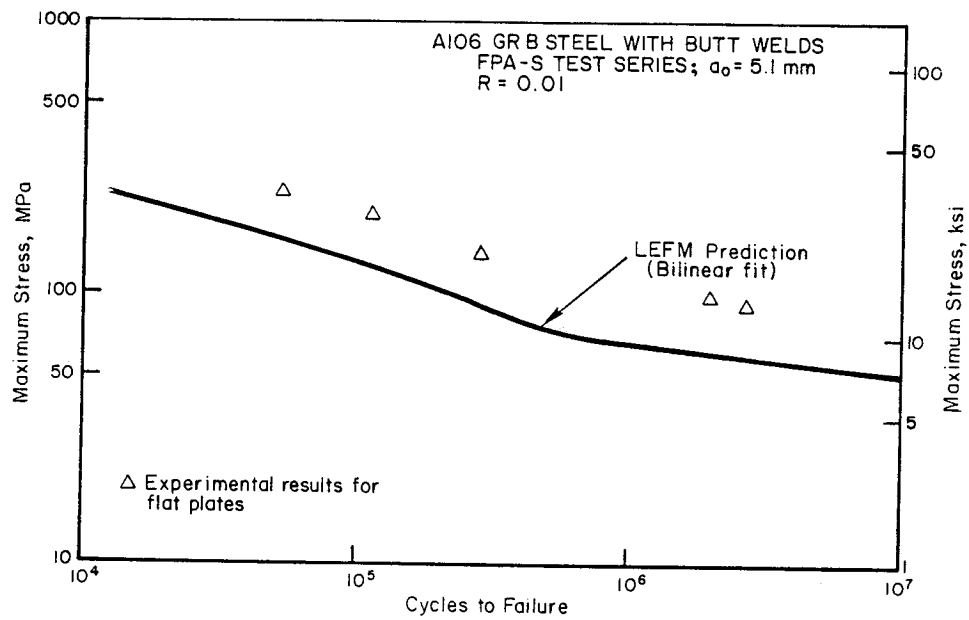


FIGURE 27. COMPARISON OF PREDICTED AND ACTUAL LIFE FOR FLAT PLATE SPECIMENS WITH $a_0 = 5.1$ MM

regime in Figure 24a. Growth rates at these low-stress levels are very low and so growth through these low growth rate regimes become the dominant fraction of the total life. Whether or not a threshold is included in using Figure 24b thus becomes a key consideration in life predictions. For the lowest stress case (FPA-S-11), use of Figure 24b without a threshold leads to predictions that are, as expected, worse than when Figure 24d which is considered to represent the threshold-like nature of the start-up transient.

In summary, the predicted fatigue life of welded flat plate specimens is consistently underestimated. The discrepancy between predicted and observed life is significant, with errors as large as a factor of ten. At stress levels tending toward the fatigue limit, the discrepancy could be reduced on a case by case basis by empirically adjusting the threshold. However, the threshold required to achieve a good fit is not unique. Note that accounting for possible stress concentration due to the backup ring would exacerbate the error--particularly at lower stress levels.

Similar calculations were performed for pipe wall segment specimens with EDM flaws. No change was made to the stress-intensity factor equation, i.e., the curved specimens were modeled as flat specimens. Corresponding predictions were also made for an "equivalent flat plate specimen" that coupled tension and bending to simulate the effect of curvature in the wall segment specimen.

The direction of the bending was given by the results of the reference experiment. The amount of bending stress at the at the outer fiber on

the equivalent flat specimen was based on the reference test for bending. It represents a realistic estimate of the bending stresses which might have been present. The results are plotted in Figure 28. Observe that the predicted lives are less than 16 to 46 percent of the actual lives for no bending and less than 5 to 11 percent with bending. That is, including bending increases the disparity between predicted and observed lives. As with the flat plate series, the predictions for the cases approaching the fatigue limit could be made to match the observed behavior by adjustment of the threshold. But, the value of the threshold is nonunique, so that such adjustments are rather artificial.

Table 9 presents a tabular summary of the predictions. The absolute difference between the actual and predicted lives is plotted against maximum stress in Figure 29. The specimens with the smallest flaws give the largest errors as a function of stress. The pipe wall segment specimens and flat plate specimens with the same flaw size give similar errors at moderate stresses. Because of the LEFM model's apparent inability to predict fatigue life with reasonable accuracy, calculations for other flaw geometries would be suspect. Therefore, further predictions were not attempted. Because the error in predictions is a function of stress for a given initial flaw size and also depends on flaw size, the LEFM analysis would not directly correlate the results. LEFM could be forced to fit the data by the use of an empirical correction that depends on both flaw size and stress. But that correction works only for the material and geometry of the specimen and flaws examined. Because this correction lacks generality, it has not been developed. Moreover, because LEFM could not be used directly to consolidate the data, a

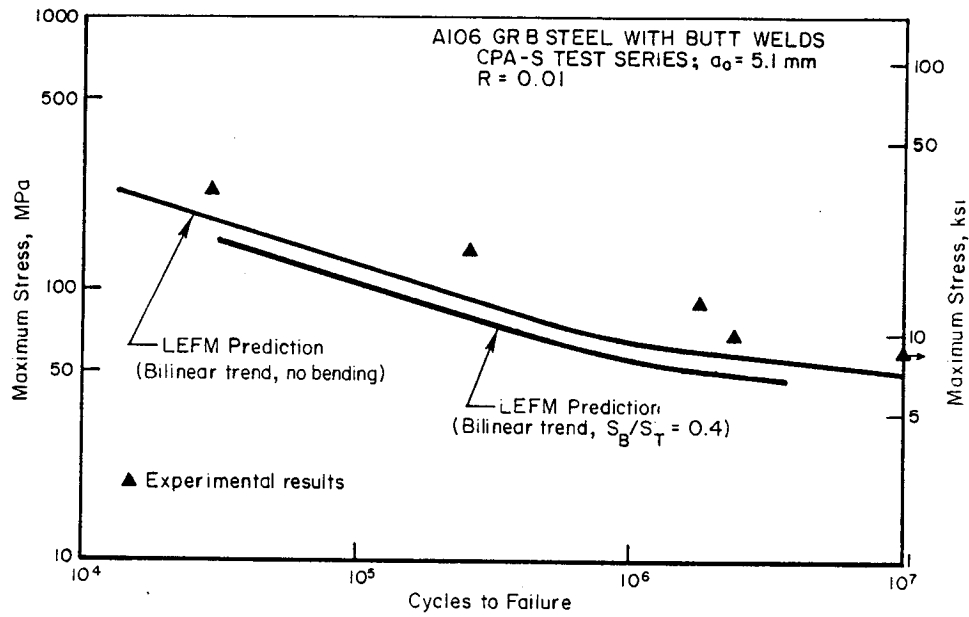


FIGURE 28. COMPARISON OF PREDICTED AND ACTUAL LIFE FOR WALL SEGMENT SPECIMENS WITH $a_0 = 5.1$ MM

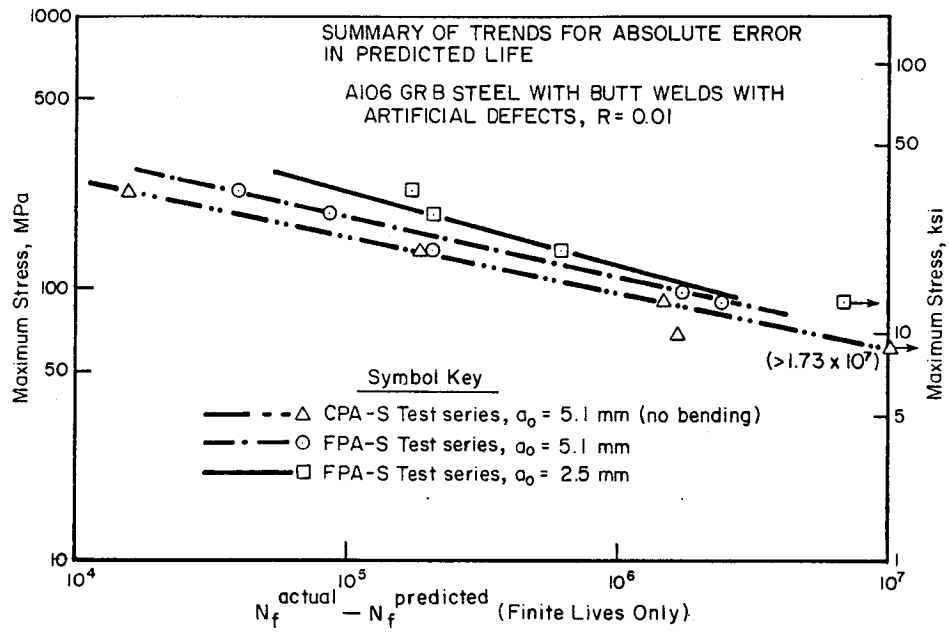


FIGURE 29. SUMMARY OF ABSOLUTE ERRORS IN PREDICTED AND ACTUAL LIFE FOR FLAT PLATE AND WALL SEGMENT SPECIMENS

TABLE 9. FATIGUE LIVES ESTIMATED USING LEFM FATIGUE CRACK GROWTH CALCULATIONS

Spec. No.	Initial Crack Depth, a		Initial Crack Semi Length, c		Maximum Stress		Actual Life, N_f^a (kilocycles)	Predicted Life N_f^P		Absolute Error $N_f^a - N_f^P$ (kilocycles)	% Error $\frac{N_f^a - N_f^P}{N_f^a} \times 100$	
	(mm)	(in.)	(mm)	(in.)	(MPa)	(ksi)		With No Bending (kilocycles)	With Bending(a) (kilocycles)		With No Bending	With Bending
FPA-S-6	2.5	(0.1)	3.8	(0.15)	228	(33.0)	234.8	60.7		174.1	74	
FPA-S-5	2.5	(0.1)	3.8	(0.15)	190	(27.5)	326.3	113.2		213.1	65	
FPA-S-10	2.5	(0.1)	3.8	(0.15)	138	(20.0)	973.8	315.2		622.6	64	
FPA-S-11	2.5	(0.1)	3.8	(0.15)	90	(13.0)	10365	3499.9		6,865.1	66	
FPA-S-14	5.1	(0.2)	7.6	(0.3)	228	(33.0)	53.2	13.2		40.0	75	
FPA-S-7	5.1	(0.2)	7.6	(0.3)	190	(27.5)	114.9	26.8		88.1	77	
FPA-S-9	5.1	(0.2)	7.6	(0.3)	138	(20.0)	287.8	79.9		207.9	72	
FPA-S-17	5.1	(0.2)	7.6	(0.3)	97	(14.0)	1980.3	257.1		1,723.2	87	
FPA-S-8	5.1	(0.2)	7.6	(0.3)	90	(13.0)	2704.3	287.6		2,416.7	89	
CPA-S-3	5.1	(0.2)	7.6	(0.3)	228	(33.0)	29.3	13.4	5.4	15.9	54	82
CPA-S-4	5.1	(0.2)	7.6	(0.3)	138	(20.0)	257.1	70.3	42.1	186.8	73	84
CPA-S-5	5.1	(0.2)	7.6	(0.3)	90	(13.0)	1814.8	324.5	194.1	1,490.3	82	89
CPA-S-8	5.1	(0.2)	7.6	(0.3)	69	(10.0)	2439.5	757.1	425.7	1,682.4	69	83
CAP-S-9	5.1	(0.2)	7.6	(0.3)	60	(8.75)	20500	1571.8		17,310.0	91	

(a) Assuming $S_{\text{bending}}/S_{\text{tension}} = 0.4$ at outer fiber of an equivalent flat plate.

fracture mechanics-type parameter has not been employed as a basis to present the data. Nor has LEFM been used to interpolate between the experimental results to examine the effect of flaw sizes or stress levels other than those for which data exist.

Commentary on the Viability of LEFM

LEFM fatigue crack growth calculations offer hope for reasonable life estimates only so long as the particular problem can be addressed adequately. As noted earlier, this involves the material FCP behavior, the applied loads, a K solution, initial defect size, and failure criteria. Each of these may contribute to the discrepancies between observed and predicted life summarized in Table 9.

The evidence of Figure 24 suggests that adequate steady state FCP data are in hand. However, the start-up transient is not addressed. The fact that the start-up transient is not addressed is significant. As stated earlier, the startup transient is a period of growth at much lower rates than Figure 24 (a or b) would suggest. Start-up transients, therefore, could account for part of the discrepancy evident in Figures 26-29 and summarized in Table 9. Indeed, because the start-up transient can be viewed as a threshold on a case by case basis, the start-up transient could influence predicted life to the same extent as a threshold. Sensitivity studies, such as [4], show small changes in threshold value can have order of magnitude effects on life for stress intensity histories near the threshold. By analogy, the start-up effect could explain rather large differences in

predicted and observed life. Reference [4] also shows changes in initial flaw size can cause large effects on predicted life. However, for the flaws under discussion, the initial size has been accurately measured. Thus small random errors in measuring initial flaw size are not considered to be a cause of the consistent discrepancies in Table 9.

The loads are not completely defined; although the axial load was controlled during the test, some bending occurred due to specimen lack of straightness. Bending stresses were shown to be quite high for the wall segment specimens. Although the amount of bending for each test was not quantified for these specimens, the direction of bending was known. Any bending of that nature would tend to shorten the predicted life--and thus increase the discrepancy with experiment.

Two additional factors can affect fatigue life, the backup ring and the weld reinforcement. The backup rings were cut in these tests. Consequently, they would be expected to have little effect on fatigue life until the cracks were large. Similarly, the weld reinforcement is expected to have little effect since it is not large enough to significantly decrease the nominal stress.

A definitive answer concerning the effect of the reinforcement cannot be given based on the work of this program. Nor can conclusions be drawn as to if and how LEFM life predictions should be adjusted to account for the effect of reinforcement.

The most obvious cause for concern over the applicability of the stress-intensity factor equation is the curvature of the pipe wall segment specimen. The fractographs of Figure 21 indicate the effect of the curvature. These fractographs show similar macroscopic trends in the growth patterns,

suggesting curvature is not a major factor. The experimental results shown in Figure 15 also indicate that the flat plates and wall segments are comparable. If the experimental results for the two kinds of specimens are similar, one would expect that the stress-intensity factor solution for the flat plate would work equally well for the curved specimen. (This assumes that any bending is properly taken into account. Another piece of evidence also suggests that the calculations done for the wall segment specimens are reasonable: the bending strains measured near the initial flaw during the check of bending reference test were relatively small, less than 10 percent of the tension strain. Thus, during the "small crack" part of the life which dominates the total crack propagation life, the crack is not subjected to high bending stresses. On the basis of the above considerations, the effect of the curvature of the pipe wall segment specimen does not preclude use of the present stress-intensity factor solution to estimate the crack propagation lives of curved specimens.

Two remaining aspects of the calculation procedure bear comment. First, the procedure for making a transition from a surface crack to a through crack obviously does not model part of the propagation life and will lead to some underestimation of the cycles to failure. However, this procedure is necessary for simplicity (the proper stress-intensity factor solutions are not available). And, the procedure employed here is commonly used in this type of analysis [5]. Second, the failure criterion (failure due to tensile rupture) agrees well with fractographic observations. The small number of cycles during which LEFM is applied to post-yield crack growth would not cause a significant underestimation of the fatigue life. (Indeed, it should cause a

slight overestimation.) The most important observation which can be made about the failure criterion's effect on estimated fatigue life is that, at the high crack growth rates experienced prior to failure, the final crack length determined from the failure criterion has a small effect on the total life.

It follows from the above discussion that there are a number of limitations to, and possible sources of error in state of the art applications of LEFM to model crack growth in weldments. Given the scope of our attempt to use LEFM as the basis for consolidation and for fatigue crack propagation calculations, the analyses should have achieved a reasonable level of accuracy. That is, errors are not expected from misapplication of the LEFM method. But, errors can be expected from the limitations of the method as applied to this problem, and in general from the variability of the experimental data to which the LEFM results are compared. For weldments, the primary limitation appears to be related to the start-up transient. For weldments made of ductile metals, the use of LEFM may be confounded somewhat by substantial elastic action at the crack-tip.

Experimental Results and Data Trends

The results of the experiments were also considered on stress-life coordinates. No attempt has been made to interpolate or extrapolate these data beyond the trend curves presented in Figures 12 through 16 and 26 through 28.

Flat plate experiments. Figure 12a presents data for four variations of the flat plate specimen. All of these specimens were tested at $R = 0.01$, and had small planar EDM flaws. Specimens 2, 3, and 4 give information about the effect of the backup ring and reinforcement. A second set of specimens, numbers 5, 6, 10, and 11, have the same flaw design, but have the weld toes ground and backup rings cut. These specimens characterize FCP in the weldment. The third variation of the flat plate geometry-- Specimen 1--was the same as the second set, except that it was ground flat to assess the effect of bending due to imperfections left after flattening. The fourth group was the same as the second group, but had a deeper flaw. These data are presented in Figure 12b.

Figure 12a shows that with the backup ring uncut, the fatigue life was extended up to about 1.5 times (compare #3 and #4 with trend for solid circles). This extended life is less than what would have been achieved if the EDM flaw had not penetrated the backup ring. (That is, if the backup ring was uncut the flaw would not be surface-connected.) This was the situation for specimen in #2. With its backup ring intact, specimen #2 exhibited a life 2.5 times longer than the reference trend (solid circles). The effect of weld reinforcement can be seen by comparing the result for specimen #1 with the reference trend. Removal of the weld reinforcement increased life by a factor of about two.

The two specimens which failed at the weld toe (#3 and #4) are also instructive. Because the backup ring pinned the crack in these specimens, the failure location shifted to the weld toe. Cracking from the weld toe initiated and became critical before an EDM flaw cut through almost one-third of

the nominal plate thickness could deepen and become critical. It appears to be remarkable that cracks initiated at the toes of ground welds before they initiated at large EDM notches. However, other investigators have found that the weld toe is often a more fatigue-sensitive location than a weld defect (Ref. 6).

Figure 12b compares the results of tests where only the initial flaw sizes differed. At short lives the trends are quite different, the lives for the larger flaw being about 0.2 times that for the smaller flaw. But, at longer lives, the trends tend to merge. Calculations indicate that this difference is not due to the initial flaw size. Table 10 presents the number of cycles predicted to cover this interval versus the actual number. (The comparison is somewhat clouded because the initial crack will not retain its original aspect ratio.) In all cases the predicted behavior is much smaller than the observed--a trend similar to that discussed earlier. Evidently, the actual crack growth occurred at a rate less than expected based on steady state response. This suggests that the EDM flaw had a startup transient or period of sharpening before it grew in a crack-like manner.

The effect of stress ratio can be seen in the results of tests for specimens with planar EDM flaws conducted at $R = 0.4$ and 0.6 , shown in Figure 13a.

Four of the five specimens did not fail solely due to the EDM flaw. As evident in Figure 18, cracks also initiated and grew from the backup ring. Crack growth from the backup ring reduced somewhat the crack growth period from the EDM flaw, so that total life is also somewhat reduced.

TABLE 10. COMPARISON OF OBSERVED AND PREDICTED CYCLE INTERVAL TO GROW FROM $A_0 = 2.5$ mm TO A DEPTH OF 5.1 mm

FPA-S Specimens		S_{mx}		Kilocycles to grow from 2.5 to 5.1 mm	
2.5 mm	5.1 mm	MPa	(ksi)	Predicted(a)	Observed
6	14	228	33	43.2	181.6
5	7	190	27.5	79.2	211.4
10	9	138	20	219.6	686.0
11	8	90	13	3105.6	7660.7

(a) Aspect ratio is somewhat higher in the tests than assumed in the calculations.

Observe from Figure 13a that, on maximum stress-life coordinates, stress ratio appears to have a significant influence on fatigue life. More than order of magnitude differences develop at the extremes of $R = 0.01$ and 0.6 at high maximum stress levels. This difference increases as maximum stress decreases. This trend is similar to that observed for smooth specimens made of carbon steel whose fatigue resistance is dominated by crack initiation. When the results of Figure 13a are replotted on stress range versus life coordinates, the data tend to collapse, but remain banded with

stress ratio. The maximum difference in life reduces to about a factor of 2.7. However, the trend is reversed from the usual pattern. These data diverge as stress increases whereas such trends usually converge to near twice the ultimate stress at short lives for specimens whose life is dominated by initiation.

Figure 13b presents the results shown on maximum stress versus life coordinates in terms of a parameter that has been shown to account for the presence of mean stress on crack initiation (or total life dominated by initiation). While a perfect correlation is not achieved, the results are consolidated into a single tight scatter band. The fact that mean stress has influence on total life is in contrast to typical results for FCP in steels. Such FCP data typically show a tight trend-free scatter band on da/dN versus ΔK coordinates at low to moderate growth rates. Therefore, Figures 13a and 13b show fatigue life is moderately dependent on stress ratio. This dependence is weaker than that characteristic of specimens dominated by crack initiation but much stronger than that typically associated with FCP.

The backup ring also played a significant role in the failure of the specimens with volumetric EDM flaws. The stress-life data presented in Figure 14 show that these specimens had lives longer than specimens tested at the same stress and flaw depth but having planar flaws. However, the fractographs in Figure 19 show that the related failures were not due to the sharpening and growth of the EDM flaws. Instead, specimens FPA-ES-1 and FPA-ES-4 failed when cracks initiating at the backup ring grew to failure (similar to the results

for $R = 0.4$ and 0.6). FPA-ES-3 failed due to cracks initiating at the intersection of the cut in the backup ring and the blind hole. None of these failures simulates weld porosity. For this reason the use of surface-connected flaws in the presence of a backup ring is an unrealistic way to simulate artificially volumetric weld defects.

Wall segment specimens. Figure 15 presented the results developed for the wall segment specimens. Two types of specimens were tested. One group had artificial (EDM) planar defects 5.1 mm (0.2 inch) deep, while the second has simulated natural planar and volumetric defects. The length of the simulated natural defects was targeted for 30.5 mm (1.2 inches) over a depth targeted for 40 percent of the wall thickness. Thus the target depth of the simulated natural defects was somewhat less than that for the artificial defect, but the length was significantly greater. Target defect areas for the case of the simulated natural defects were about 30 percent greater than that for the EDM defects.

Figure 15a indicates there is little difference between the flat plate data and the wall segment data for an initial flaw size of 5.1 mm. The difference that exist is easily explained by the bending in the CPA-S series specimens.

Examination of Figure 15a shows two data points that lie well off the data trend. In the case of specimen number 2 this occurs because the flaw was inadvertently omitted even though the backup ring was cut. This result shows that the presence of the 5.1 mm deep flaw reduces the life by about a

factor of 10. In the case of specimen number 6 the cutting of the backup ring was inadvertently continued well into the specimen. For this case the 5.1 mm defect had little effect on the life which was controlled by cracking through the thickness from the entire length of the long shallow defect associated with cutting beyond the backup ring. The figure shows the life is reduced by a factor of 10 for this case as compared to growth from the 5.1 mm defect.

Results for the simulated natural defects were shown on Figure 15b, in comparison with the trend for the results for artificial flaws in flat and wall segment specimens. Observe that the scatter in these data is increased as compared with the EDM data. Note too that the results for the natural defects are bounded by the results for artificial defects, with two exceptions. As might be expected the trend of the data for volumetric defects lies at lives longer than for planar defects. However, the difference in lives for volumetric and planar defects is not as great as was expected. For the data developed it is less than an order of magnitude.

The fact that the natural defects lie at lives longer than the artificial defects is significant. It means that, even though the natural defect areas are larger, the natural defects are less effective as crack starters as compared to EDM defects. That is, the period of sharpening or startup transient for the natural defects is longer than for the EDM defects.* In turn, this means that artificial defects can be used to develop lower bound estimates of the behavior of actual defects. Observe in Figure 15b that three data points are well off the trends. For specimens 9 and 4 in the CPN series,

* Residual stresses are not a major factor since specimens are normalized prior to testing. However, the wake of plasticity may be different in that microstructures are different near the defects.

inspection of the fractographs in Figures 22 and 23 shows the presence of defects much larger than desired. In contrast, specimen 2 in the CPN series failed to develop the desired level of porosity.

Vessel experiments. Figure 16 presents the results of vessel tests for welds with artificial and natural defects. The target defect covered a shallow part circular area developed over 120 degrees. The depth was about 60 percent through the nominal wall thickness, quickly decreasing to zero depth at the ends. The maximum depth is about 40 percent of the thickness if the reinforcement is included. The area fraction of this defect is about 20 percent of the nominal axial crosssection, compared to about 13 percent for the flat plate and wall segment specimens with the large defects. Examples of the cross sectional area covered by these defects were shown in Figure 23b. Artificial defect shape and size could be controlled reasonably to achieve depths close to the target. However, for natural defects only partial porosity or LOF was achieved in the target area. Actual levels of LOF and porosity developed represent perhaps one-third of the target level. Also, the simulated porosity and LOF lies on weld beads or bevelled material, and thus was not on the plane of maximum principal stress. The area of the natural defects was about 20 to 50 percent of that for the artificial defects.

Examination of Figure 16a shows that volumetric artificial defects survived from 4 to 8 times longer than similar sized planar artificial defects. This difference, which was less than anticipated, is controlled by how the planar and volumetric defects were developed. Figure 9 shows that the volumetric defect was really just a planar defect with a blunt tip. As such

the difference in lives for this comparison may be much less than would occur for true planar and volumetric defects. Thus, as with the flat plate specimens, the method used for developing volumetric artificial defect was not adequate.

Figure 16a also provides for comparison of results for simulated planar natural defects and planar artificial defects. Observe from the figure that none of the vessel tests designed to generate data for natural planar defects produced failure at the defect. Instead, as detailed in Table 8, failure at other welds terminated these tests. Consequently, each of the data points for the natural planar defects carries an arrow to denote that failure did not occur. Comparison of the trends for open and solid circles shows that the natural defects survive from 4 to 20 times longer than their artificial counterparts. This situation develops for cases where the artificial defects are in some cases much larger than their natural counterparts. Thus, the increased fatigue resistance of the natural defects is not surprising. This pattern is in strong contrast to the results for natural and artificial wall segment specimens (CPN vs CPA in Figure 15b). These data showed that somewhat larger natural defects survived a little longer than did the smaller artificial defects.

Direct comparison of the trend for natural planar defects in curved segments and vessel tests is not possible since absolute defect area* (and aspect ratio) to produce comparable lives are very different. Likewise,

* The relative defect area is about a factor of four larger in the vessel as compared to the flat plate with $a_0 = 2.5$ mm (trend curve in Figure 13b). The corresponding relative aspect ratios differ by about a factor of 14.

direct comparison with artificial planar defects is not possible. But, it is clear comparing the results for wall segments ($R = 0.01$) shown as the trend line in Figure 16a with the data for the vessels ($R = 0.1$) that defect size is a dominant consideration in developing acceptance criteria. Correcting for the small difference in stress ratio in the manner of Figure 13b does not alter this fact, as is evident in Figure 16b.

In terms of LEFM the range of initial stress intensity factor at the deepest location for the artificial planar defect in the vessels is between 11.1 (12.34) and 12.8 (14.23) MPa \sqrt{M} (ksi \sqrt{in}) at a maximum pressure of 10 MPa (1450 psi) and a stress ratio of 0.10*. This range of stress intensity factor scales as maximum pressure range. Thus, the initial values of ΔK can be found by reference to Table 8 for each of the vessel tests. Such calculations show that the initial values of ΔK are in the range $10.66 \leq \Delta K \leq 21.85$ MPa \sqrt{M} for the extremes in the two K solutions. Corresponding initial values of the range of initial stress intensity factor for the segment specimen bound

* The ranges of stress intensity factor represent solutions for the vessel geometry and initial flaw size based on [7] and [8], respectively. Biaxiality in the vessel is not considered to be a factor since stresses parallel to the crack don't have a big effect on growth rate for conditions where the plastic zone is small compared to specimen and crack dimensions.

the experiments in the CPA series that were done at maximum stresses from 90 to 138 MPa.

The lives for the CPA series fall in the interval 2.5×10^5 to 1.8×10^6 for the just noted stresses.

If the ΔK histories were the same in the vessel and the segment tests, LEFM analysis indicates that vessel tests and CPA tests would have comparable growth periods. Figure 16b shows that the lives for comparable Δk levels in the segment and vessel specimens were not even close. The corresponding observed lives for the vessels fall in the interval from 5×10^4 to 4×10^5 --about a factor 4 less than for the CPA series. The difference in critical crack sizes (leak in the vessels versus limit load in the specimens) might account for this difference. However, analysis indicates that the correction for this difference in life is about an order of magnitude smaller than required. Vessel biaxiality can be dismissed as a source of this disparity based on LEFM analysis. Differences in residual stress cannot be invoked to explain this result since all specimens have been normalized prior to testing. As with the earlier results it appears that a difference in the start up transients must exist. Thus it seems that segment specimens do not relate directly to vessel test (pipe) behavior. Empirical corrections could be developed to deal with the higher stress cases. However, for stress levels and flaw sizes that involve start-up transients this correction may be uncertain.

DEVELOPMENT OF DEFECT ACCEPTANCE CRITERIA

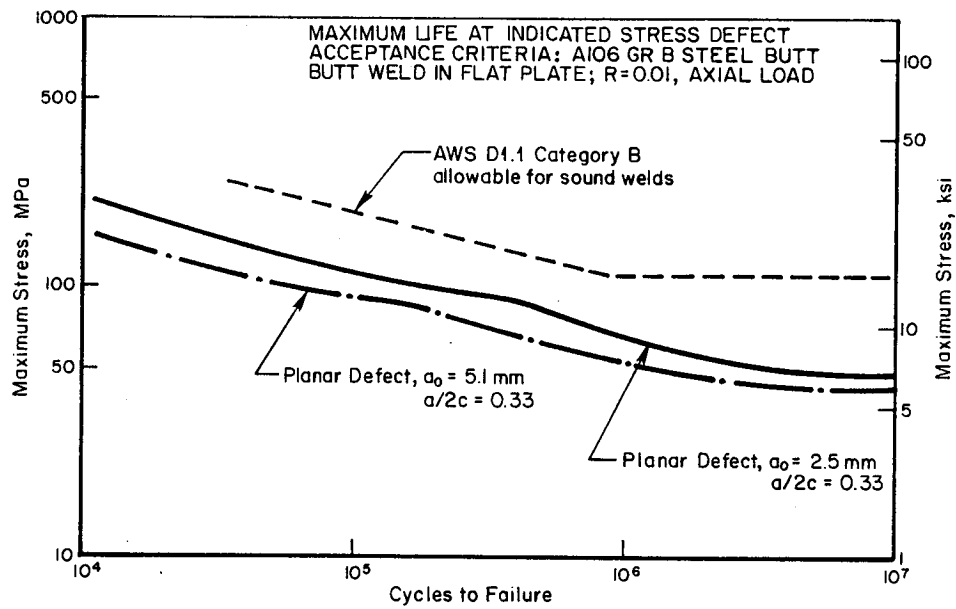
The ANSI/ASME piping code designated B31.3 relates the allowable stress for sound welds to the specified minimum yield stress (SMYS). Yield stress depends on the temperature. Accordingly, the B31.3 code lists allowable stresses for A106 GR B as a function of temperature. For the situation at hand the B31.3 code lists an allowable stress of 137.8 MPa (20 ksi). The ANSI/AWS D1.1 code lists allowable stresses for fatigue for nonredundant structures without regard to the type of steel. Pipe welds, which are butt welds, fit into the AWS system of weld categories as Category B. The allowable stress for this category is characterized by a mathematical power law at lives less than 8×10^5 cycles, and as a constant equal to 110.2 MPa (16 ksi) at longer lives. The limits for these codes corresponding to infinite life operation have been shown on all S-N data plots on the left-hand scale.

The AWS code tends to bound safely all data for lives less than 10^6 cycles developed for flat and wall segment specimens, including results for the flaw depth of 5.1 mm. However, beyond the life of 10^6 cycles the reduction of the fatigue limit due to the flaw means that the code allowable for sound welds is nonconservative. The B31.3 code is overly conservative at short lives. However, at short lives general allowables are not governed by fatigue so this conservatism is anticipated. At lives in excess of about 3×10^5 cycles the B31.3 code for sound welds becomes nonconservative--again because of the effect of the defect.

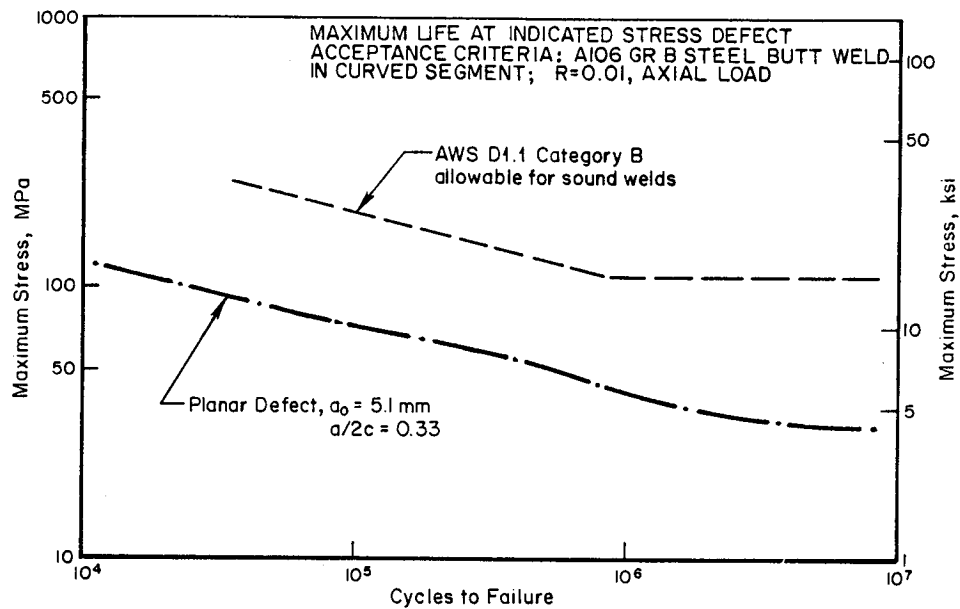
The ASME Boiler and Pressure Vessel (BPV) code and the AWS code include provisions that define a sound weld. These provisions are based on workmanship standards. Pressure system codes stipulate that indications not meeting these standards must be repaired. To this end defect acceptance criteria for code rejectable indications must be developed.

The data developed in this study can be used to define such criteria for selected geometries and defect types and sizes. The criteria based on the data developed, however, does not provide for scatter in properties, nor do they cover a wide range of flaw sizes. For this reason, a factor of safety should be applied. The choice of the factor of safety is usually based on past experience. The uncertainty involved in the design allowable also should be considered. For the present, scatter and uncertainty in stress can be accounted for reasonably by applying a safety factor of 2 on stress or 20 on life, whichever is greater. (These are the safety factors used in the design curves for the ASME BPV code.) These factors will be applied directly. Because of (1) the sensitivity of life to flaw size and aspect ratio, and (2) the fact that uncertainty in this parameter varies greatly case by case, no factor of safety is applied to crack depth. This factor should be assessed case by case and the lower bound result applied. Finally, the failure criterion depends on section width and thickness. The acceptance criteria reflect results for the section sizes and nominal thickness investigated. Judgment should be exercised in adding or subtracting life accordingly.

Figure 30 presents defect acceptance criteria including the 2 and 20 factor of safety. Part a of this figure represents axial loading of flat plate butt welds. Parts b and c represent butt welds under axial loading in curved segments and pressurized vessels (pipes), respectively. Note that the

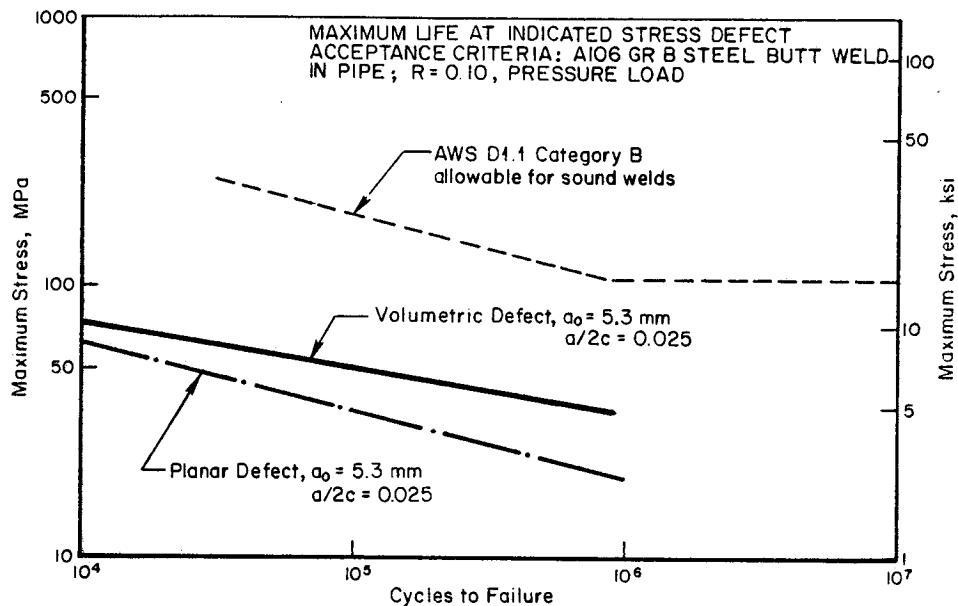


a. Axially loaded flat plates



b. Axially loaded curved segments

FIGURE 30. DEFECT ACCEPTANCE CRITERIA FOR BUTT WELDS
IN A106 GRB STEEL



c. Pressure loaded pipe

FIGURE 30. (Concluded)

criteria for vessels does not include the possibly significant effects of secondary bending and weld induced residual stresses. These acceptance criteria represent the specified flaw sizes for the test sections used. In all cases the acceptance criteria lie well below current code allowables for sound welds, except for B31.3 at very short lives.

LEFM could be used to interpolate between or extrapolate beyond the trends in Figure 30 for other flaw sizes and aspect ratios. But in light of Figure 29 this is an uncertain adventure. Figure 29 emphasizes that the error encountered in using LEFM in the present application is a function of stress level. Also, the slopes of the trends and the level below which the error tends to become very large depend on the flaw size. (While not shown the

error probably depends on aspect ratio.) It follows from Figure 29 that the error also depends on crack size.

Note that the criteria presented in Figure 30 represent artificial planar defects in specimens tested at a constant stress ratio. The artificial planar defects represent a lower bound to the simulated natural defects and so contain some inherent conservatism. Since planar defects were a lower bound for the limited volumetric results in this study and the literature, the trends also could be used for volumetric defects of a similar size. Mean stress effects could be accounted for by using the techniques described in the discussion of Figure 13b. The data could be replotted in terms of the mean stress damage parameter or stress range for this purpose. Finally, note that these criteria deal specifically with A106 GR B steel. If, as implied within the AWS D1.1 criteria for sound welds, the behavior of a defective weld in a given category behave similarly in a range of steels, these defect acceptance criteria can be applied to other steels. However, recognizing that the sharpening behavior will depend on the steel, care should be exercised in such extrapolation. Particular care should be taken for applications to steels with very different chemistries and strength levels.

SUMMARY AND CONCLUSIONS

This three-phase study was directed at developing a fitness for service defect acceptance criteria for welds with defect indications. The study focussed on A106 GR B steel pipe. The first phase involved a literature search and critical review to develop preliminary acceptance criteria to the extent permitted by the data. The second phase developed data for flat plate, wall segment, and vessel specimens containing artificial or natural planar or volumetric defects. The final phase developed acceptance criteria from the test data.

The criteria developed represent specific combinations of material, geometry, flaw type and size, and loading. Attempts to use state of the art LEFM to predict the behavior of the combinations studied showed the analysis underestimated observed behavior. Errors approaching a factor of 10 in life were not uncommon, and would have been greater had complications such as bending and stress concentrations not been ignored. In light of these errors LEFM has not been used to interpolate between the data generated and that already in the literature. The results developed suggest that designs based solely on LEFM may contain a large factor of safety. While desirable, excessive safety factors imply excessive materials and fabrication costs, and increase the volume of weld deposit, the cost of inspection, and the probability that the weld will contain undetected defects. Thus, while state of the art LEFM can be used to assess durability, some work is warranted to understand causes of significant disparity between predicted and observed fatigue resistance.

A number of conclusions have been drawn and observations noted throughout this report. These conclusions and observations must be taken in light of the specimens, flaws, and test techniques used in this study. Two aspects make the data developed particularly unique. First, the desire was to examine the influence of defect shape and size over a range of specimen geometries. To this end the uncertain influence of variable residual stresses was avoided by normalizing all specimens prior to testing. In turn data analyses were simplified. Second the desire was to examine axially stressed piping. No attempt was made to include secondary bending stresses.

The more significant conclusions follow along with pertinent observations.

- (1) There is an apparent start-up transient associated with the early growth of a defect. The duration and significance of this transient appears to depend on stress level, defect type (natural vs artificial and planar vs volumetric), and defect size (and aspect ratio).
- (2) The start-up transient appears to occupy a major fraction of specimen life in that state-of-the-art linear elastic fracture mechanics analysis of rather simple specimen and flaw geometries estimated poorly the life spent in propagation assuming that the defect was crack-like from the first loading cycle. The exact cause of the start-up effect is not clear. Either defects take time to develop a sharp tip or

the initial wake of plasticity (closure) differs from a long steady-state wake or some combination are plausible sources of the start-up effect.

- (3) Flat plate and wall segment specimens show similar fatigue resistance for otherwise identical flaw geometry and stress history.
- (4) Vessels show a fatigue resistance reduced from that anticipated based on flat plate or wall segment specimens with rather similar histories of the range of the stress intensity factor. Conservative empirical correlations could be used to predict vessel (pipe) response from the results of simpler specimens, except at low stress where this approach may be uncertain.
- (5) Fitness for service criteria could not be directly developed for vessels (pipe) from simpler specimen results, even with the help of linear elastic fracture mechanics.
- (6) Defect acceptance criteria should be based on experiments using material and test specimen and defect configurations similar to the in-service application.
- (7) Rather long and deep planar defects were not as deleterious as was a slight code acceptable undercut at the toe of the weld reinforcement for both flat

plate and wall segment specimens. More effort should be directed towards understanding why the start-up transient is shorter for such surface flaws as compared to planar defects. Fracture mechanics tied to far-field elastic stress adds little insight in this situation.

REFERENCES

1. Leis, B. N., "An Energy Based Fatigue and Creep-Fatigue Damage Parameter", J. Press. Vess. Tech. ASME, Vol. 99, No. 4, 1977, pp 524-533.
2. Newman, Jr., J. C., "A Review and Assessment of the Stress Intensity Factors for Surface Cracks", Part-Through Crack Fatigue Life Prediction, ASTM STP 687, J. B. Chang, Editor, ASTM 1979, pp 16-42.
3. Newman, Jr., J. C. , and Raju, I. S., "An Empirical Stress-Intensity Factor Equation for the Surface Crack", Engineering Fracture Mechanics, Vol. 15, No. 1-2, pp 185-192, 1981.
4. Leis, B. N. and Mayfield, M. E., "Influence of Initial Defect Distribution on the Life of the Cold Leg Piping System", in Mechanics of Nondestructive Testing, Plenum Press, 1980, pp 325-342.
5. Part-Through Crack Fatigue Life Prediction, ASTM STP 687, J. B. Chang, Ed., ASTM, 1979.
6. Yung, Y.-Y., and Lawrence, F. V., "Analytical and Graphical Aids for the Fatigue Design of Weldments", Fitness for Purpose in Welded Construction Conference, May 14-16, 1985.
7. Lim, E. Y., Dedhia, D. D., and Harris, D. O., "Approximate Influence Functions for Part-Circumferential Interior Surface Cracks in Pipes", Fracture Mechanics: 14th Symposium - Volume I: Theory and Analysis, ASTM STP 791, J. C. Lewis and G. Sines, Eds., American Society for Testing and Materials, 1983, pp I281-I296.
8. Kumar, V., German, M. D., and Shih, C. F., "An Engineering Approach for Elastic-Plastic Fracture Analysis", EPRI NP-1931, July, 1981.

APPENDIX A: HIGHLIGHTS FROM INTERIM REPORT NUMBER 1

DEVELOPMENT OF A RATIONALE FOR ACCEPTANCE OF WELDS HAVING CODE-REJECTABLE DEFECTS

INTRODUCTION

The purpose of this program is to develop a rationale for accepting welds containing workmanship-based code-rejectable defects. This development is planned to evolve through three phases of study. Efforts of the first phase--the technical literature is to be reviewed to determine the effects of planar and volumetric defect indications on fatigue life data--is highlighted in this Appendix.

Activities in the first phase were designed to generate a preliminary acceptance criterion for volumetric and planar indications. These activities were timed such that this preliminary criterion would be available early in the program for two reasons. First, a preliminary criterion would aid in selecting (1) test parameters like load (stress) level, (2) specimen geometries, (3) sizes and shapes of artificial and natural weld defects, and (4) indicate favored schemes to generate artificial and simulate natural weld defects. Second, the existence of a preliminary criterion might aid in the process of recertification of the Langley physical plant.

Unfortunately, as has been documented in the monthly and quarterly reports, the volume of data anticipated based on the apparent worldwide Fitness for Purpose (FFP) activity was not realized. Indeed, only one primary data source--the University of Illinois, and two secondary sources--the University of Tennessee and the Canadian Center for Mineral and Energy

Technology (CANMET) responded to formal requests for data. For this reason, the first phase did not develop the scope of the database anticipated nor did it attempt to develop criteria, since most of the information provided is not of the type of data required. Consequently, this appendix only highlights an overview of the approach taken to acquire data, and outlines the plan of action taken as a fall-back position.

THE APPROACH

The approach to acquire the necessary data involved several steps

- (1) identify potential data sources
- (2) establish availability of the data and interest in making it available
- (3) preliminary correspondence on data requirements, and
- (4) correspondence including a questionnaire and data documentation forms.

The approach was established with the concurrent of the monitor. Its implementation, which likewise was with the concurrence of the monitor, involved the following steps

- (1) a machine search
- (2) a series of telephone calls, telex's and letters, and
- (3) follow-up telephone calls, telex's and letters.

RESULTS

The machine search involved three major data bases--METADEX (Metals Abstracts), WELDASEARCH, and MCIC. Nineteen key words and phrases were used

in various combinations. These included: fitness for service/purpose, weld(s), defects(s), fatigue, fracture, crack (with initiation), crack (with propagation), steel(s), metal, acceptance, criteria, quality, crack(s), flaw(s), lack of fusion, lack of penetration, porosity, volumetric, planar. Several combinations of these words were run to narrow the literature to that specifically of interest to this study. One combination produced over a 1000 hits, clearly suggesting a potential wealth of data existed. The combination was narrowed further, but this still produced over 500 hits. Finally, the combination was restricted to information specifically related to weld defect acceptance criteria. As a result, the field was narrowed to 27 hits, of which the descriptions indicated only about ten (not counting apparent duplications) met the needs of this study. These included work done in Germany, Norway, Napan, Russia, France, Canada, the United Kingdom, and the United States. Of these, several were in their native language, and were excluded from further consideration on that basis. However, when addresses were available, the authors were independently contacted by mail, as part of our mail and phone campaign.

It is noteworthy that while the list of key words is extensive, certain articles known to exist were not identified as part of the machine search. Such a result, while surprising, is not uncommon in machine searches.

DATA ACQUISITION CAMPAIGN

The machine search did identify a number of focal points for the research on defect acceptance criteria. The list of key individuals and organizations includes mainly the Europeans and the Japanese, as is evident in

Table A1. Each of these individuals has been contacted using one or more of several approaches, depending on cost and convenience.

The telex presented as Exhibit I was used as the first point of contact. The telephone also served as the basis for first point of contact in several cases. Follow-up to the first point of contact was in the form of Exhibit II. Responses of interest to Exhibit I came only from the Canadians (CANMET and their Welding Institute), Carle Lundin (University of Tennessee), Bill Munse and Fred Lawrence (University of Illinois), and Paul Rabbe (Creusot-Loire). There were even fewer indications of genuine interest in the form of detailed responses to Exhibit II. Only CANMET and the University of Illinois agreed to send data, whereas the Welding Institute of Canada (WIC) expressed continuing interest. Phase I closed without generating a useful database.

To date, data indirectly useful have been received from CANMET and the University of Illinois. The best information is cited here as Reference A1. Results presented in that report suggest that acceptance criteria for defects can be developed using the plan adopted for this program. As expected, volumetric defects behaved somewhat differently than did planar defects. Finally the results developed showed that acceptance criteria differed depending on the material under consideration.

The machine search also identified two recent comprehensive survey/reviews of fatigue of weldments. These are noted as References A2 and A3. These surveys did not contain original data and results of direct interest. But they did examine the subject of acceptance criteria in the manner typical of papers included in References A4-A15. Because information found in the two surveys and in References A4-A15 precluded manipulation to

TABLE A1. LIST OF KEY CONTACTS

Dr. S. Maddox and
Dr. H. Harrison
The Welding Institute
Abington Hall
Cambridge U.K. CB1 6AL

Dr. M. B. Kasen
National Bureau of
Standards
Boulder, Colorado 80303

Dr. A. Glover
Weld Institute of
Canada
391 Burnamthorpe Rd
Oakville Ontario L6J 6C9
Canada

Mr. P. Rabbe
Crusot Loire
Centre de Recherches
Dunieux
Firminy France

Mr. R. Hellen
Berkeley Nuclear Laboratories
Gloucestershire, England

Dr. S. Usami
Hitachi Research Laboratory
Hitachi Ltd.
3-1-1, Saiwai-cho
Hitachi-shi, Japan

Dr. M. Kawahara
Technical Research Center
Nippon Kokan K.K.
Kawasaki, Japan

Dr. M. Ishihara
Hiratsuka Research Laboratory
Sumitomo Heavy Industries
Hiratsuka Japan

Dr. Sandor
Sun Ship Inc.
Chester, Pennsylvania 19013

develop criteria, or was incomplete and therefore prone to misinterpretation, virtually all of the information received could not be used in direct support of criteria development to suit the purpose of this study.

IMPLICATIONS OF THE DATA ACQUISITION CAMPAIGN

Evidently, the lack of response to our campaign stemmed from the fact that NASA, through Battelle (or for that matter, most others in North America) have nothing to bring to the table in exchange for the detailed data sought . Accordingly, until Battelle has developed the data for A106B piping following the proposed program plan; it is unlikely that existing data will be made available.

Study of Reference A1 indicates that criteria are materials specific. Results for the mild (construction) steel reported therein can be used as a guide for sizing flaws and choosing test parameters for the present program. For this reason, testing had to be planned to move more cautiously, at least early on, until some feel for the suitability of the flaw geometries and sizes, and test parameters was developed. Throughout the experiments, changes were discussed with the program monitor to obtain his concurrence with test parameters.

SUMMARY

Data anticipated to exist have not been forthcoming. Fortunately, however, enough data exist to (1) indicate the approach adopted for data generation in this program will be successful (2) determine sizes and types of defects and (3) establish how to recreate these defects in actual welds.

REFERENCES

- A1. Bowman, M. D., and Munse, W. H., "The Effect of Discontinuities on the Fatigue Behavior of Transverse Butt Welds in Steel". Report UILU-ENG-81-2006, The Civil Engineering Department, University of Illinois, April, 1981.
- A2. Lundin, C. D., "The Significance of Weld Discontinuities--A Review of Current Literature: WRC Bulletin 222, The Welding Research Council, December, 1976.
- A3. Booker, M. K., Booker, B. L. P., Meier, H. B., and Hueschkel, J., "Fatigue of Weldments in Nuclear Pressure Vessels and Piping". NUREG/CR-1351, ORNL/NUREG-64, February, 1980.
- A4. Fitness for Purpose in Shipbuilding, 1st National Conference, Boulder, Colorado, October, 1980--ed. L. W. Sandor, U.S. Department of Commerce, Maritime Administration.
- A5. Welding Research in the 80's, Proc. Int. Conf. Osaka Japan, October, 1980, Osaka Welding Institute.
- A6. Tolerance of Flaws in Pressurized Components, Proc. Conf. Institute of Mechanical Engineers, London, U.K., May, 1978.
- A7. Criteria for Preventing Service Failures in Welded Structures, Proc. 3rd International Symposium, Tokyo 78, Japanese Welding Society.
- A8. Fitness for Purpose in Welding Construction, Proc. Int. Conf., May, 1982, American Welding Society.
- A9. Pipeline Welding and Inspection, Proc. Conf. September, 1982, American Welding Society.
- A10. Fitness for Purpose Validation of Welded Construction, November, 1981, The Welding Institute, U.K., Proc. Int. Conf.
- A11. Pipeline Welding in the 80's Proc. Specialist Symposium, 1981, Australian Welding Research Association.
- A12. Pipeline and Energy Plant Piping, Proc. International Conference, November, 1980, Pergamon.
- A13. Developments in Pressure Vessel Technology, Applied Science Publ., 1979.
- A14. International Institute of Welding of Welding - Public Session, 1979, Proc., published by the Institute, London Eng., 1979.

EXHIBIT I: TELEX

We are under contract to experimentally develop Fitness for Purpose defect acceptance criteria for fatigue failure of welds in piping. A literature search indicates your name/organization is prominent in this field.

This telex solicits related raw data in exchange for corresponding data for comparative evaluations. If you are interested in such an exchange, please indicate so by telex as soon as possible. Details on the program and data required will follow.

Thank you for your timely response.

Regards,

Brian N. Leis

BNL/kf

EXHIBIT II: DATA SUMMARY SHEET FOR WELDS WITH INDICATIONS

1. Material Properties/Characterization:

a. Material:

b. Heat Treatment:

c. E:

BM

WM

HAZ

d. Yield Strength, 0.2% S_y :

e. Ultimate Strength, S_u :

f. Hardness (indicate kind):

g. Red. in Area, % RA:

h. Strain Hard. Exp., n :

i. Strength Coeff., K :

Please provide cyclic properties if available:

j. Cyclic Yield Strength, 0.2% S_y' :

k. Cyclic Strain Hard., n' :

l. Cyclic Strength Coeff., K' :

Please provide either stress-life data, strain-life data, or the following:

m. Fatigue Strength Coeff., σ_f' :

n. Fatigue Ductility Coeff., ϵ_f :

o. Fatigue Strength Exp., b :

p. Fatigue Ductility Exp., c :

Please provide data for the BM:

q. Plane Strain Fracture Toughness, K_{IC} :

r. Long Crack Threshold Stress Intensity:

s. Crack Growth Coefficient, A:

t. Crack Growth Exponent, m.

u. Grain Size for BM, WM, and HAZ: BM

WM

HAZ

v. Comments (chemistry, microstructure):

c. Were residual stress measurements made? (Y or N):

Comments:

d. Other comments on inspection

7. Flaw Characteristics

a. Natural or Artificially Induced:

b. Method of Introducing Flaw:

c. Type of Flaw (circle words describing initial flaw):

lack of fusion/penetration slag and porosity through crack

surface crack embedded crack other _____

d. General Shape (elliptical, etc.):

e. Location in Weld (sketch):

f. Initial Flaw Length and/or Depth (may be indicated or sketch above):

g. Comments:

8. Number of Cycles Spent Sharpening Flaw to 0.1 - 0.5 mm.

9. Crack Measurement and Growth

a. Measurement Technique:

Accuracy:

Precision:

b. Quantity Measured (a and/or 2c):

c. Were plots made of flaw size to cycle number? (Y or N)

If yes, please attach.

d. Were plots made of flaw growth rate to flaw size or K? (Y or N):

If yes, please attach.

Note: Please include experimental data points as well as trend curves.

e. Definition of K:

10. Stress-life Data for Welds with Indications

a. Please attach stress- or strain-life plots; as above, experimental data points as well as trend curves are needed.

b. Definition of Failure:

11. Please include anything else you believe relevant including other analysis, acceptance criteria, etc.

12. Reference(s) in which this data appeared:

Was any additional data added to the published data?

Standard Bibliographic Page

1. Report No. NASA CR-178114		2. Government Accession No.		3. Recipient's Catalog No.	
4. Title and Subtitle The Influence of Defects of the Fatigue Resistance of Butt and Girth Welds in A106B Steel				5. Report Date July 1986	
				6. Performing Organization Code	
7. Author(s) B.N. Leis, D.P. Goetz and P.M. Scott				8. Performing Organization Report No.	
				10. Work Unit No.	
9. Performing Organization Name and Address Battelle Columbus Division 505 King Avenue Columbus, OH 43201 BD96-1734				11. Contract or Grant No. NAS1-17404	
				13. Type of Report and Period Covered Contractor Report	
12. Sponsoring Agency Name and Address National Aeronautics and Space Administration Washington, DC 20546				14. Sponsoring Agency Code 323-53-71	
15. Supplementary Notes Langley Technical Monitor: C. Michael Hudson Final Report					
16. Abstract This three-phase study was directed at developing a fitness for service defect acceptance criteria for welds with defect indications. The study focussed on A106 Gr. B steel pipe. The first phase involved a literature search and critical review to develop the preliminary acceptance criteria to the extent permitted by the data. The second phase developed data for flat plate, wall segment, and vessel specimens containing artificial or natural planar or volumetric defects. The final phase developed acceptance criteria from the test data.					
17. Key Words (Suggested by Authors(s)) welds, fatigue, acceptance criteria, defects, porosity, slag, lack-of-penetration, lack-of-fusion, cracks, fitness for purpose, A106B steel, startup transient, closure				18. Distribution Statement Unclassified - Unlimited Subject Category 26	
19. Security Classif.(of this report) Unclassified		20. Security Classif.(of this page) Unclassified		21. No. of Pages 107	
				22. Price A06	

For sale by the National Technical Information Service, Springfield, Virginia 22161

